# E-cadherin mediated Apical Membrane Initiation Site localisation

Xuan Liang[1], Antonia Weberling[1], Chun Yuan Hii[1], Magdalena Zernicka-Goetz[1,2], Clare E Buckley[1#]

[#] Corresponding author

[1] Department of Physiology, Development and Neuroscience
University of Cambridge, Downing Street
Cambridge CB2 3DY, UK
ceb85@cam.ac.uk

[2] Division of Biology and Biological Engineering
California Institute of Technology
1200 E. California Boulevard, Pasadena, CA, 91125, USA

**Character count:** 51,039 characters including spaces, excluding title page, references and figure legends.

## Abstract

Individual cells within *de novo* polarising tubes and cavities must integrate their forming apical domains into a centralised apical membrane initiation site (AMIS). This is necessary to enable organised lumen formation within multi-cellular tissue. Despite the well documented importance of cell division in localising the AMIS, we have found a division-independent mechanism of AMIS localisation that relies instead on Cadherin-mediated cell-cell adhesion. Our study of *de novo* polarising mouse embryonic stem cells (mESCs) cultured in 3D suggest that cell-cell adhesion localises apical proteins such as PAR-6 to a centralised AMIS. Unexpectedly, we also found that mESC cell clusters lacking functional E-cadherin still formed a lumen-like cavity in the absence of AMIS localisation but did so at a later stage of development via a 'closure' mechanism, instead of via hollowing. This work suggests that there are two, interrelated mechanisms of apical polarity localisation: cell adhesion and cell division. Alignment of these mechanisms in space allows for redundancy in the system and ensures the development of a coherent epithelial structure within a growing organ.

**Keywords:** AMIS/Cadherin/apical-basal polarity/epithelial tube/*de novo* polarisation

## Introduction

Most organs in the body arise from tubes or cavities made from polarised epithelial cells. These cells have a strict apico-basal orientation; they align their apical ends along a centrally located lumen. Some tubes, such as the anterior neural tube in amniotes, arise via folding and closure of an already polarised epithelial tissue, through mechanisms such as actomyosin-mediated apical constriction (Nikolopoulou *et al*, 2017). However, many tubes and cavities, such as the posterior neural tube, mammary acini, kidney tubules and mammalian epiblast arise via apical-basal polarisation within the centre of an initially solid tissue. The mechanisms by which such '*de novo*' polarisation is coordinated within dynamically growing tissue has been the focus of a significant body of research from several different models and have relevance both for understanding polarity-associated diseases and for directing organ bioengineering approaches.

Although the exact mechanisms are still under debate and may differ in different epithelia (Buckley & Johnston, 2022), Laminin, Integrin β1 and RAC1 signalling from the extra cellular matrix (ECM) is now well established to be necessary for directing the overall apico-basal axis of polarisation of internally polarising tubes (Akhtar & Streuli, 2013; Bedzhov & Zernicka-Goetz, 2014; Buckley *et al*, 2013; Molè *et al*, 2021; Bryant *et al*, 2014; Yu *et al*, 2004). What is less clear is how the precise localisation of the apical membrane initiation site (AMIS) is directed at the single cell level and how this is coordinated between neighbouring cells. The AMIS is a transient structure, marked by the scaffolding protein Partitioning-defective-3 (PAR-3) and tight junctional components such as Zonula occludens-1 (ZO-1), that defines where apically targeted proteins will fuse with the membrane, therefore determining where the lumen will arise (Bryant *et al*, 2010; Blasky *et al*, 2015). It is important that the subcellular localisation of the AMIS is coordinated between cells during morphogenesis to enable organised lumen formation.

The current literature suggests that cell division plays an important role in AMIS localisation. In particular, the post-mitotic midbody has been shown to anchor apically directed proteins (Wang *et al*, 2014; Li *et al*, 2014; Rathbun *et al*, 2020; Luján *et al*, 2016; Schlüter *et al*, 2009). However, studies within the zebrafish neural rod showed that, whilst misorientation of cell division results in disruption of the apical plane at a tissue level, these phenotypes can be rescued by inhibiting cell division (Tawk *et al*, 2007; Zigman *et al*, 2011; Quesada-Hernandez *et al*, 2010; Ciruna *et al*, 2006). We also previously demonstrated that individual zebrafish neuroepithelial cells were able to recognise the future midline of the neural primordium and organise their intracellular structure around this location in advance and independently of cell division. This resulted in the initiation of an apical surface at whichever point the cells intersect the middle of the developing tissue, even if this is part way along a cell length (Buckley *et al*, 2013). This suggests that, while cell division is undoubtably a dominant mechanism, there must be another overlying mechanism driving AMIS localisation during *de novo* polarisation. The earliest indication of midline positioning in the zebrafish neural rod was the central accumulation of the junctional scaffolding protein Pard3 (PAR-3) and the adhesion protein N-cadherin (Buckley *et al*, 2013; Symonds *et al*, 2020). This led us to hypothesise that cell-cell adhesions could direct the site for AMIS localisation during *de novo* polarisation. In line with this hypothesis, β-catenin mediated maturation of N-cadherin was found to be necessary for the recruitment of the PAR apical complex protein atypical protein kinase C (aPKC) in the chick neural tube (Herrera *et al*, 2021). Opposing localisations of ECM and Cadherin proteins were also found to be sufficient to specify the apical-basal axis of hepatocytes in culture (Zhang *et al*, 2020).

To test the role of cell-cell adhesions in AMIS localisation, we turned to mouse embryo stem cell (mESC) culture in Matrigel, which has been used as an *in vitro* model for the *de novo* polarisation of the mouse epiblast (Bedzhov & Zernicka-Goetz, 2014; Shahbazi *et al*, 2017; Molè *et al*, 2021; Kim *et al*, 2021). This allowed us to study the initiation of apico-basal polarity of embryonic cells alongside the first cell-cell contacts between isolated cells and small cell clusters. It also allowed us to determine within a mammalian model whether division-independent polarisation is a conserved feature of *de novo* polarising structures. Unlike vertebrate epithelial cell culture models such as Madin-Darby canine kidney (MDCK) cells, which initiate lumenogenesis as early as the 2-cell stage when cultured in Matrigel (Bryant *et al*, 2010; Blasky *et al*, 2015), mESC cells in Matrigel only form lumens at the multicellular stage after 48-72 hours in culture, coinciding with an exit in pluripotency (Bedzhov & Zernicka-Goetz, 2014; Shahbazi *et al*, 2017). This results in a

relatively clear separation of the stages of *de novo* polarisation (Fig 1A). Previous literature suggests that the AMIS is formed at the 2-cell stage, around 24-36 hours after culture in Matrigel, as denoted by membrane-localised PAR-3 and ZO-1 and sub-apical localisation of apical proteins such as Podocalyxin (PODYXL) (Shahbazi *et al*, 2017). The pre-apical patch (PAP) stage is formed after 36-48 hours in culture, as denoted by the fusion of apical proteins such as PODXYL, PAR-6 and aPKC to the apical membrane and the displacement of junctional proteins PAR-3, ZO-1 and E-cadherin to the apico-lateral junctions (Shahbazi *et al*, 2017; Kim *et al*, 2021), following which lumenogenesis is initiated after 48-72 hours in culture.

To determine the role of cell division and of cell adhesion in mESC AMIS localisation, we analysed mESC cells cultured in Matrigel at the AMIS stage with and without cell division in wild type and E-cadherin knock out cell lines. We then further analysed polarisation and lumenogenesis in the absence of E-cadherin. Our results suggest that there is a division-independent mechanism of AMIS localisation that relies instead on E-cadherin mediated cell-cell adhesions.

## Results

### Cell division is dispensable for AMIS localisation

First, we tested whether cell division was necessary for AMIS localisation in mESC rosettes. We cultured naïve, unpolarized mESCs (ES-E14 cells) in 2D on gelatin with 2i/LIF and then treated them with mitomycin C to block cell division. We then isolated single cells and seeded them into Matrigel without 2i/LIF, in N2B27 differentiation medium (Fig 1B). Cell divisions were efficiently blocked during the first 24 hours post seeding, during which time individual cells contacted each other and formed cell clusters in the absence of cell division (Movie EV1, Fig EV1A,B).

To assess AMIS localisation, we carried out immunofluorescence (IF) for PAR-3 and ZO-1 at 24hrs post seeding. As previously published (Shahbazi *et al*, 2017), in addition to several puncta at the cell peripheries, both PAR-3 and ZO-1 localised to the membrane at the centre of control cell-cell contacts, marking the AMIS in the majority of cell clusters (Fig 1Ci,Hi). Interestingly, division-blocked cells also localized PAR-3 and ZO-1 to the central membrane (Fig 1Cii,Hii, quantified in Fig 1D-G & I). In both control and division-blocked cell clusters, there was a small proportion that had not yet fully localised the AMIS at the 24-hour stage (Fig 1D,I), where PAR-3 was either not localised (Fig S1A) or was only weakly present at cell-cell interfaces (Fig S1B). E-cadherin was upregulated along the whole length of the cell-cell interfaces in both dividing and non-dividing cell clusters, with a higher level of E-cadherin at the cell-cell interface relative to the cell-matrix interface (Fig 1C, EV1C). To quantify the subcellular localization of PAR-3 in each cell cluster, we carried out intensity profiles across the cell-cell interface of 2-cell doublets (Fig 1Ea, F) and calculated the ratio between centralised and surrounding non-centralised PAR-3 in multi-cellular clusters (Fig 1Eb, G). This confirmed that PAR-3 localised to a small central area at the cell-cell interface in both control and division-blocked 2-cell doublets and multi-cellular clusters. Golgi apparatus and centrosomes were also localised to the centre of cell-cell contacts both in dividing and non-dividing conditions (Fig 1H-K), confirming that mESCs were polarised in the absence of cell division. mESC clusters also centrally localised PAR-3, ZO-1 and polarised the Golgi apparatus when cell division was blocked using an alternative compound, aphidicolin (Fig EV1D-H).

Together, these results demonstrate that cell division is dispensable for *de novo* AMIS localisation in polarizing mESCs.

**Cell-cell contact directs PAR-6 localisation**

To understand the dynamics of apical protein polarisation in the absence of cell division, we generated a mESC stable cell line expressing mCherry-PAR-6B and imaged cells live. In line with previous characterisation of PAR-6 by IF (Shahbazi *et al*, 2017; Kim *et al*, 2021) in control dividing cells, mCherry-PAR-6B localised to the apical membrane by the PAP stage at 48 hours and to the luminal apical membrane from 72 hours (Fig 2A and S2B). In addition, the transgene allowed us to better visualize PAR-6B puncta at earlier 24h AMIS stages of development. At this stage, mCherry-PAR-6B was localized sub-apically, polarized to towards the central region of cell-cell contact (Fig 2A and S2B). Some mCherry-PAR-6B puncta appeared to be associated with the Golgi network. However, a large proportion of mCherry-PAR-6B was in the cytoplasm sub-apically (Fig S2C), suggesting that PAR-6B puncta were in the process of being delivered to the apical membrane at 24 hours. A similar polarised distribution of PAR-6B was observed in both control and division-blocked cells (Fig 2B,C, S2C), demonstrating that cell division is dispensable for apical protein polarisation.

We next assessed the dynamics of PAR-6B polarisation. In both control and division-blocked cells, non-cortical mCherry-PAR-6B puncta were visible at the single cell stage. In control cells, these puncta relocalised to the abscission plane, following cell division (Fig 2D, S2D, Movie EV2). In division-blocked cells, PAR-6B puncta dynamically relocalised to newly forming cell-cell contacts, eventually forming cell-cell clusters with centrally localised PAR-6B (Fig 2D, S2E, Movie EV2).

These results suggest that cell-cell contact directs PAR-6B localisation at the central AMIS, independent of cell division.

**E-cadherin adhesions are necessary for AMIS localisation**

The above results suggest that there is a division-independent mechanism of AMIS localisation that relies instead on cell-cell adhesions. Since E-cadherin is the predominant adhesion molecule in non-neural epithelia, we hypothesised that it might be important in AMIS localisation. To achieve a full removal of E-cadherin, we employed an *E-cadherin* knock-out (*Cdh1* KO) mESC line (Larue *et al*, 1996).

To assess AMIS localisation, we again carried out IF for PAR-3 and ZO-1 at 24hrs post seeding. As seen earlier (Fig 1), both PAR-3 and ZO-1 localised to the central region of cell-cell contact within wild-type (W4 cells) doublets/clusters with and without division. However, PAR-3 and ZO-1 localisation was strongly inhibited in the absence of E-cadherin (Fig 3A-D & G,H). RNAi knock-down (KD) of E-cadherin in ES-E14 mESCs showed similar results to the *Cdh1* KO mESCs: PAR-3 at the central region of E-cadherin KD two-cell clusters was significantly reduced (Fig S3B-D).

To investigate AMIS localisation at a single cell level, we co-cultured division-blocked wild type (ES-E14) and *Cdh1* KO cells and analysed division-blocked chimeric mESC doublets, comprising one control and one

*Cdh1* KO cell. Whilst homogenous control doublets localised PAR-3 to the central region of the cell-cell interface, heterogeneous chimeric doublets did not localise PAR-3 centrally (Fig 3E,F). The same result was seen in E-cadherin RNAi chimeric doublets (Fig S3Bb). Golgi and centrosome localisation towards the cell-cell interface suggested that the overall axis of polarity was maintained, even in the absence of both cell division and E-cadherin (Fig 3G-I & S3D). These results demonstrated that E-cadherin is necessary for AMIS localisation.

Since E-cadherin is localised along the whole cell-cell interface but PAR-3 and ZO-1 localise at central cell-cell interfaces, we next used fluorescence recovery after photobleaching (FRAP) to compare the stability of E-cadherin protein at central and side regions in 2-cell mESC clusters (Fig EV2C). E-cadherin immunofluorescence (Fig EV2A, B) and E-cadherin-eGFP (Fig EV2D) levels were the same at these two regions. However, FRAP of E-cadherin-eGFP showed that the mobile fraction of E-cadherin-eGFP was lower in the central region than the side regions (Fig 3J, K). Therefore, E-cadherin junctions are more stable at the centre-most region of the cell-cell interface, which may provide at least a partial explanation for why AMIS localisation occurs precisely at this region.

It has previously been demonstrated that a reduction in E-cadherin can slow pluripotency exit (Soncin *et al*, 2009). However, pluripotency exit was previously shown not to alter AMIS formation (Shahbazi *et al*, 2017). In support of these results, we also found that cells maintained in the pluripotent state when cultured in Feeder cell medium provided with 2i/LIF still localised the AMIS, with and without cell division (Fig EV3A-C). However, in line with our results showing lack of AMIS localisation in *Cdh1* KO cells cultured in the absence of 2i/LIF (Fig 3), cells cultured in the presence of 2i/LIF also could not localise an AMIS in the absence of E-cadherin (Fig EV3A-C). Despite this result, we wanted to check whether the stage of pluripotency exit differed between WT and *Cdh1* KO cells in our experiments since this might indicate a different speed of maturation. We therefore carried out IF for Orthodenticle Homeobox 2 (OTX2) protein, which is necessary for pluripotency exit, and the pluripotency marker protein Nanog. Although, as expected, the overall level of nuclear OTX2 increased and Nanog decreased over the 24-hour course of development, we found no significant difference in post-mitotic levels of OTX2 and Nanog between WT and *Cdh1* KO cells (Fig EV3D). This result suggests that there was no difference in the stage of pluripotency exit in the cell clusters that we analysed during this study, and this is therefore unlikely to play a role in the lack of AMIS localisation seen in *Cdh1* KO cells.

These results demonstrate that E-cadherin adhesions between cells are necessary for AMIS localisation but not for the overall axis of polarity. They also demonstrate that ECM in the absence of E-cadherin is insufficient for AMIS localisation.

**Adhesion molecules P-cadherin, JAM-A and Nectin-2 are not necessary for AMIS localisation**

E-cadherin is not the only form of adhesion molecule that is expressed at cell-cell contacts. A complex network of interactions between the PAR-complex, adhesion molecules, MAGUK scaffolding proteins and the actin cytoskeleton is responsible for building cell-cell junctions (Buckley & Johnston, 2022). Of relevance to this study, PAR-3 has been found to directly bind to transmembrane Junctional Adhesion Molecules (JAMs) and Nectin proteins in mammals (Ebnet *et al*, 2001; Takekuni *et al*, 2003; Itoh *et al*, 2001). In the

mammalian embryo, JAM-A and Nectin-2 adhesion molecules are expressed between inner cell mass cells in the mouse blastocyst (Thomas *et al*, 2004). We found that JAM-A and Nectin-2, as well as P-cadherin, were expressed at cell-cell contacts in 2D cultured mESCs (Fig EV4A).

We therefore carried out IF of 2-cell mESC clusters cultured in Matrigel for 24 hours to determine the localisation of P-cadherin, JAM-A and Nectin-2 at the AMIS stage. Whilst the majority of 2-cell and 4-cell clusters formed a polarised PAR-3 centre, P-cadherin was uniformly expressed along cell-cell interfaces (Fig 4A & EV4B). JAM-A was uniformly expressed along cell-cell interfaces at the 2-cell stage (Fig 4D) and concentrated toward the centre of 4-cell mESC clusters (Fig EV4C). At the 2-cell stage, Nectin-2 was expressed along the whole cell-cell interface with a sight concentration towards the central regions where PAR-3 was localised (Fig 4G). At the 4-cell stage, Nectin-2 was concentrated toward the centre of the clusters (Fig EV4D). These results suggest that PAR-3 localises at the AMIS before JAM-A or Nectin-2.

Next, we used siRNA KD of protein function in dividing and division-blocked cells to test whether P-cadherin, JAM-A or Nectin-2 proteins were necessary for AMIS localisation. However, following siRNA for each of these proteins, PAR-3 was still polarised to the centre of cell-cell contacts (Fig 4 and EV4B-D). Compared to the loss of PAR-3 polarisation upon E-cadherin KO or KD (Fig 3, S3), the results demonstrate that P-cadherin, JAM-A and Nectin-2 are not necessary for AMIS localisation. Indeed, when the centralised PAR-3 localisation was lost in the the E-cadherin KO mESC 2-cell clusters (Fig 3A-C), P-cadherin, JAM-A and Nectin-2 were still expressed at the cell-cell interface between the mESCs (Fig EV4E-G). This suggests that E-cadherin based adhesions might be specifically responsible for mediating AMIS localisation.

**E-cadherin adhesions are sufficient to initiate AMIS localisation, independent of ECM signalling and cell division**

As discussed, ECM-mediated signalling plays an important role in orienting the axis of polarisation within *de novo* polarising systems. Recently, the apico-basal axis of cultured mature hepatocytes was established by a combination of ECM signalling and immobilised E-cadherin (Zhang *et al*, 2020). However, PAR-3 has also recently been shown to polarise in mESCs lacking functional Integrin-β1 or cultured in agarose in the absence of ECM proteins (Molè *et al*, 2021). Our current study shows that the AMIS can localise in the absence of cell division but not in the absence of E-cadherin. We therefore wanted to explore the relative roles of ECM, cell division and E-cadherin in AMIS localisation.

We first eliminated the influence of ECM by culturing division-blocked mESCs (ES-E14) in 0.5% agarose and carried out IF for PAR-3 after 30 hours in culture. These cells were still able to polarise PAR-3, even in the absence of both cell division and ECM proteins (Fig 5A,B). However, in line with our earlier results (Fig 3), PAR-3 localisation was strongly inhibited in *Cdh1* KO cells (Fig 5A,B). These results suggest that AMIS localisation occurs independently of both ECM signalling and of cell division, relying instead on E-cadherin.

To further test the sufficiency of E-cadherin adhesions in initiating AMIS localisation, we cultured individual division-blocked mESCs (ES-E14) onto either E-cadherin recombinant protein or Fibronectin pre-coated glass, then topped the cells with N2B27 medium, with or without 20% Matrigel and carried out IF for PAR-3 after 24 hours in culture. Like results from hepatocytes (Zhang *et al*, 2020), cells plated on E-cadherin and

topped with Matrigel localised PAR-3 to the centre of the cell-cadherin interface (Fig 5C-F). However, this central PAR-3 localisation was significantly reduced when cells were plated on fibronectin (Fig 5C-F). Interestingly, cells cultured on E-cadherin but in the absence of Matrigel still localised PAR-3 to the centre of the cell-cadherin interface (Fig 5C-F).

These results demonstrate that E-cadherin adhesions are both necessary and sufficient for initiating AMIS localisation, while ECM is not necessary or sufficient for AMIS localisation.

**E-cadherin is necessary for hollowing lumenogenesis**

We next wanted to test the importance of E-cadherin-mediated AMIS localisation in lumenogenesis. We therefore cultured WT (ES-E14) and *Cdh1* KO mESCs and fixed them at the AMIS 24-hour stage, PAP 48-hour stage and lumen 72 and 96-hour stage. We then carried out IF for PAR-3 and ZO-1 to label AMIS/apical-lateral junctions and PODXYL to label apical proteins. Whilst most WT cell clusters had a centralised apical domain or small lumen after 48 hours in culture, very few *Cdh1* KO cell clusters had made a centralised apical domain by the 48-hour PAP stage (Fig 6A-D). In line with our earlier findings at the 24-hour AMIS stage (Fig 3), this provides further evidence that E-cadherin is necessary for centralised AMIS localisation. However, we noticed that a small percentage of *Cdh1* KO cell clusters at 48 hours had formed an open 'cup-shape', with apically localised PODXYL (Fig 6B) and apico-laterally localised junctional PAR-3 (e.g. Fig 6Aiii) and ZO-1 (Fig EV5A). We termed these 'open cavities' (Fig 6C). Surprisingly, by the 72-hour lumen stage, approximately 75% of *Cdh1* KO cell clusters had formed polarised cavities, approximately 50% of which were open cavities and 50% were closed (Fig 6D,E). Over the course of 48-96 hours in culture, the overall percentage of polarised cavities increased (Fig 6D) as did the proportion of these structures that were 'closed' (Fig 6E). This suggested that these cavities might form via gradual 'closure' of the tissue, rather than via hollowing. Both 'open' and 'closed' cavities were surrounded by polarised Golgi apparatus, demonstrating that the overall apico-basal axis of cells was in-tact. (Fig EV5B).

To further assess the morphogenetic mechanism by which cavities form in *Cdh1* KO cells, we generated WT (ES-E14) and *Cdh1* KO mESC lines labelled with LifeAct-mRuby (Fig S4). We visualised the process of lumenogenesis within mESCs cultured in Matrigel via live imaging (Fig 6F and Movies EV3, 4). This confirmed that, whilst the WT cell clusters made a central lumen (8/8 movies on day 2) and then expanded this already central lumen (8/8 movies on day 3), *cdh1* KO cell clusters first generated an open cup-shape cavity (3/3 movies on day 2), which then gradually closed, eventually generating a centralised lumen-like structure without hollowing at a later stage of development (3/3 movies on day 3).

These results demonstrate that, in the absence of E-cadherin mediated AMIS localisation, cell clusters do not hollow but instead generate lumen-like cavities via a closure mechanism (Fig 7). Our results also demonstrate that E-cadherin and centralised AMIS localisation are not required for apical membrane formation. In the absence of E-cadherin, an apical surface is still formed but this occurs later in development so appears less efficient.

**Discussion**

**Epithelial cells can polarise *de novo* in the absence of cell division.**

Both AMIS associated proteins PAR-3/ZO-1 and apical polarity protein PAR-6B localised similarly in WT and division-blocked mESCs (Figs 1 and 2). This finding supports our previously published zebrafish neuroepithelial cell *in vivo* analysis, which demonstrated the division-independent localisation of Pard3 (PAR-3) and ZO-1 at the neural rod primordial midline (Buckley *et al*, 2013). Together, this demonstrates that although division is an important contributor to AMIS formation, a division-independent mechanism of *de novo* polarisation and AMIS localisation can occur in both *in vivo* and *in vitro* conditions. Whilst disorganised lumen formation can also occur in the absence of division in the zebrafish neural rod (Buckley *et al*, 2013), this was not possible to test within the mESC culture model since mitomycin treated cell clusters did not survive beyond 30 hours in culture.

**E-cadherin based cell-cell contacts are necessary and sufficient to initiate AMIS localisation**

AMIS localisation in *Cdh1* KO cell clusters is strongly inhibited (Fig 3) and individual mESC cells can localise their AMIS to the central region of the cell-cadherin interface independently from ECM-signalling (Fig 5). Together this demonstrates that formation of E-cadherin-based cell-cell contacts is both necessary and sufficient for initiating AMIS localisation and that ECM is insufficient to direct AMIS localisation in the absence of E-cadherin. Our results therefore suggest that Cadherin-based cell-cell adhesion may provide the spatial cue required for AMIS localisation during *de novo* polarisation. This in turn localises apical proteins such as PAR-6B to a centralised region of cell-cell contact (Fig 2), determining where the lumen will arise.

Whilst we demonstrate that AMIS localisation can occur independently from cell division, the importance of abscission and midbody formation in apical protein targeting has been robustly demonstrated and the molecules involved are now starting to emerge (Schlüter *et al*, 2009; Wang *et al*, 2014; Rathbun *et al*, 2020; Luján *et al*, 2016; Klinkert *et al*, 2016; Mangan *et al*, 2016; Li *et al*, 2014; Wang *et al*, 2021). Rather than acting as the initial symmetry breaking step in AMIS localisation, we suggest that tethering of apically directed proteins to the midbody might instead act to transiently align cell division, cell adhesion and the forming apical domain, therefore enabling an organised structure to be generated in the presence of dynamic cell movement and tissue growth (Buckley & Johnston, 2022). The localisation of scaffolding and tight junction-associated proteins such as PAR-3 and ZO-1 at the AMIS might aid in this alignment. For example, Cingulin is a tight junctional protein that has been shown to bind both to the midbody and to FIP5, which is important for the apical targeting of vesicles containing apical proteins (Mangan *et al*, 2016). During zebrafish neural rod development, cell adhesion and cell division align to allow an organised structure to arise from dynamically reorganising cells (Symonds and Buckley 2020) and loss of N-cadherin results in mis-oriented cell divisions and a disrupted apical domain (Zigman *et al*, 2011). Once apical proteins fuse with the apical membrane, proteins associated with junctions such as Cadherin, PAR-3 and ZO-1 are then cleared from the apical surface and instead form the apical-lateral junctions, as demonstrated in several different epithelial systems (Symonds *et al*, 2020; Morais-de-Sa *et al*, 2010; Kim *et al*, 2021).

Whilst we have demonstrated that E-cadherin directs AMIS localisation, we do not yet have a full explanation for why AMIS proteins localise at the central-most point of cell-cell contact in the absence of divisions, despite E-cadherin localisation all along the cell-cell interface. As mentioned, PAR-3 has been shown to

directly bind to the transmembrane JAMs and Nectin proteins (Ebnet *et al*, 2001; Takekuni *et al*, 2003; Itoh *et al*, 2001). However, these proteins localised to the AMIS later than PAR-3 and were not necessary for AMIS localisation (Fig 4). PAR-3 and PAR-6 have been found to be directly recruited to Cadherin proteins within endothelial cells (Iden *et al*, 2006). Recently, opposing actin flows in migrating cells as they first encounter each other were found to be responsible for regulating the first AJ deposition via tension-mediated unfolding of a-catenin and further clustering of surface E-cadherin molecules (Noordstra *et al*, 2021). Together, this could provide an explanation for how the first contacts between cells could act as an apical 'seed', therefore defining the position of the AMIS within multicellular tissues. This could therefore explain why we have previously seen an upregulation of N-cadherin at the zebrafish neural rod midline, where cells growing from either side of the organ primordium meet (Symonds *et al*, 2020). However, it is still unclear how this might regulate the subcellular localisation of the AMIS to the centre of cell-cell contacts. Our FRAP results demonstrate that E-cadherin is relatively more stable at the central-most point of contact between two adhering cells (Fig 3J, K). This might suggest that E-cadherin is more stably bound via its downstream partners to the internal actin cytoskeleton at this point, which might help to stabilise or to localise AMIS proteins. In line with this hypothesis, previous publications have demonstrated an upregulation of phosphorylated MYOSIN-II (pMLC) at the AMIS (Molè *et al*, 2021), which is suggestive of higher actomyosin-mediated tension. Uncovering the mechanisms directing adhesion-dependent AMIS localisation precisely to the midpoint of cell-cell adhesions will be an interesting area for future studies. In addition, a recent study of chick neural tube polarisation (where N-cadherin is the dominant Cadherin) has demonstrated that the interaction of β-catenin with pro-N-cadherin in the Golgi apparatus is necessary for the maturation of N-cadherin, which is in turn important for apical-basal polarity establishment (Herrera et al, 2021). This provides the possibility that the polarised Golgi apparatus that we observe in the mESC clusters might be directionally delivering mature E-cadherin to the central-most region of cell-cell contact.

**In the absence of an AMIS, lumens form via 'closure' rather than hollowing**

The centralised localisation of an AMIS appears necessary to enable lumen hollowing within multi-cellular clusters. *Cdh1* KO cells lack AMIS localisation at the 24-hour AMIS stage (Fig 3). However, they still retain their apico-basal polarity axis (as denoted by Golgi apparatus and centrosome localisation, Fig 3G-I) and form apico-lateral junctions at luminal stages of development (Fig 6). Therefore, *Cdh1* KO cells do appear to still make an apical membrane (presumably directed by ECM-mediated signalling) but do so more slowly than in WT cells and without going through a centralised AMIS stage. This suggests that the role of E-cadherin in *de novo* polarisation is specifically to localise the AMIS, which enables the integration of individual cell apical domains to a centralised region preceding lumen hollowing. The lack of a centralised AMIS in E-cadherin deficient cells could also explain the multiple-lumen (but otherwise polarised) phenotypes previously seen in E-cadherin deficient MDCK cells cultured on collagen (Jia *et al*, 2011). Although the other adhesion molecules we have tested (P-cadherin, JAM-A and Nectin-2) did not contribute to centralised AMIS formation, mESCs cultured in Matrigel and mouse inner cell mass cells only become fully epithelialised and start to generate the central cavity once they have exited pluripotency and there are multiple cells in the structures (Kim et al., 2021; Shahbazi et al., 2017). Thus, whilst E-cadherin appears to be essential for AMIS localisation, other adhesion molecules may be important at later polarisation and lumenogenesis stages.

A surprising observation was the ability of *Cdh1* KO mESC clusters, in the absence of AMIS localisation, to instead form 'lumen-like' structures via a 'closure' process. Our movies of *Cdh1* KO cell clusters (Movies EV3 & 4) confirmed conclusions from fixed data (Fig 6) that *Cdh1* KO cell clusters first generate a polarised, open cup-shape cavity, before 'closing'. Due to phototoxicity, we only had limited sample size and movie lengths, thus we were not able to fully exclude the possibility that the hollowing lumenogenesis occurs to some small extent in parallel, but our data is not suggestive of hollowing lumenogenesis in the *Cdh1* KO cell clusters. We do not currently know the mechanism by which such 'closure' occurs in *Cdh1* KO cell clusters. However, the presence of F-actin and p-MLC rich cable-like structures in 'cup'-shaped open cavities is potentially suggestive of a contractile process (Fig EV5). Understanding the relative roles of mechanics in localisation of the AMIS and in 'opening' vs. 'closing' tubes is an important future research goal, as is the potential role of cell geometry in mediating such differences. Additionally, collective cell migration could play a role in this 'closure' mechanism. Collective inwards migration of cells caused lumen formation via a folding mechanism when MDCK monolayers were overlaid with a soft collagen gel (Ishida *et al*, 2014). A similar collective process could be occurring in the *Cdh1* KO cell clusters from our study, which were cultured in a soft (10%) Matrigel and formed loosely connected cell clusters, which then 'closed' to make a centralised lumen.

In summary, our work suggests that Cadherin-mediated cell-cell adhesion directs AMIS localisation during *de novo* polarisation of epithelial tubes and cavities. Our work also suggests that ECM is insufficient to direct AMIS localisation in the absence of Cadherin. In parallel with the well described role of the midbody in tethering apical proteins, this suggests that there are two, interrelated mechanisms of AMIS localisation: cell adhesion and cell division. The alignment of these cellular processes allows for redundancy in the system and provides an explanation for how an organised epithelial structure can arise within the centre of a proliferating organ primordium.

## Material and Methods

### Cell cultures and treatment

mESC carriers were maintained in Feeder Cell medium in Corning cell culture dishes precoated with 0.1% Gelatin (ES-006-B, Sigma-Aldrich), at 37 □ suppled with 5% $CO_2$ at one atmospheric pressure. The culture medium was renewed every three days. The cells were trypsinised when reaching confluency to be passaged or subjected to experiments. The cells were regularly checked to be mycoplasma-contamination-free.

For 3D culture of wild-type and E-cadherin knock-out mESCs, 20 µL of Matrigel (356231, Corning, Lot 354230, 354234, 356231) was spread evenly to the bottom of each well in a µ-slide 8 well dish (80821, Ibidi). The dish was left on ice for 10 minutes to flatten the Matrigel surface, then was left at 37 □ for 10 minutes to solidify the Matrigel. mESCs were trypsinised, pipetted thoroughly and passed through a cell strainer (431750, Corning) to isolate cells into single cells. Singled mESCs were suspended in the N2B27 medium and seeded onto the solidified Matrigel. The seeded density was: control, 14 cells/$mm^2$; mitomycin

C treated, 227 cells/mm$^2$. The cells were left at 37 □ for 15 min when over 95% of the cells attached to the Matrigel, then the culture medium was renewed to 10% Matrigel/N2B27 medium with or without 2i/LIF.

For control and *Cdh1* KO mESC chimeric cluster cultures, wild-type and *Cdh1* KO mESCs were mixed at 1:4 ratio and co-cultured in 2D in the Feeder Cell Medium. They were then treated with mitomycin C for 2 hours, trypsinized and seeded for 3D Matrigel culture at 227 cells/mm$^2$.

For mESC cultured in agarose, 5,000 control or 125,000 mitomycin C treated cells were suspended in a 37 ℃ warmed 20 µL 0.5% low melting point agarose (16520, Invitrogen) droplet at the bottom of the µ-slide 8 well dish. The dish was left at room temperature for 5 minutes to solidify and topped with the N2B27 medium. The cells were then cultured at 37 □, 5% $CO_2$ until analysis.

For cells cultured on E-cadherin and fibronectin coated glass, the µ-slide 8 well dish was incubated with nitrocellulose/methanal at 37 □ for 3 hours and left to air dry. The dish was then incubated with 40 µg/mL mouse E-cadherin recombinant protein (8875-EC-050, Bio-Techne) or 40 µg/mL fibronectin (F1141, Sigma-Aldrich) at 4 □ overnight. The dish was briefly washed with water. Mitomycin C pre-treated ES-E14 cells were seeded onto the dish at 14 cells/mm$^2$ in N2B27 medium. The cells were allowed to attach to the glass at 37 □ for one hour, then the medium was renewed to N2B27 medium with 20% Matrigel. The cells were fixed 24 hours post Matrigel introduction.

For mitomycin C treatment, the cells were incubated with 10 µg/mL mitomycin C (J63193, Alfa Aesar) in culture media at 37 □ for two hours. The mitomycin C contained media were removed and the cells were washed with PBS briefly. Then the mitomycin C treated cells were trypsinised and subjected to further experiments.

Mouse PAR-6B coding DNA sequence (cDNA, GenBank: BC025147.1) was assembled with mCherry by Gibson assembly, LifeAct-Ruby cDNA were sub-cloned from an existing pRN3P-LifeAct-Ruby plasmid. The cDNAs were cloned into pDONR221 plasmid and introduced into the PB-Hyg-Dest plasmid using Gateway technology (Thermo Fisher Scientific). The PB-Hyg-Dest-mCherry-PAR-6B or the PB-Hyg-Dest-LifeAct-Ruby plasmid was co-transfected with the piggyBac plasmid using Lipofectamine 3000 to generate Hygromycin B resistant stable cell lines. The mCherry-PAR-6B or LifeAct-Ruby expressing mESC stable cell line was created via 10 µg/mL Hygromycin B selection and single cell colonies expansion. Primers used for cloning are listed below:

| |
|---|
| **Forward: attB1-N-mCherry** |
| 5-GGGGACAAGTTTGTACAAAAAAGCAGGCTTCGCCACCATGGTGAGCAAGGG-3 |
| **Reverse: C-mCherry-N-PAR6B** |
| 5-TGCCGGTGGCCGCGGTTCATCGGATCCCCCGGGCTGCAGGA-3 |
| **Forward: C-mCherry-N-PAR6B** |
| 5-TCCTGCAGCCCGGGGGATCCGATGAACCGCGGCCACCGGCA-3 |
| **Reverse: C-PAR6B-attB2** |
| 5-GGGGACCACTTTGTACAAGAAAGCTGGGTCTAGCAGATGATGTCGTCCTCGT-3 |
| **Forward: attB1-N-LifeAct** |
| 5-GGGGACAAGTTTGTACAAAAAAGCAGGCTTCGAAGGAGATAGAACCATGGGCGTGGCCGACCTGAT-3 |
| **Reverse: C-mRuby-attB2** |
| 5-GGGGACCACTTTGTACAAGAAAGCTGGGTGTTACCCTCCGCCCAGGCCGG-3 |

455

456 **Compositions of cell culture media**

457

458 Feeder Cell Medium: DMEM (41966, Thermo Fisher Scientific), 15% FBS (ES-009-B, Sigma-Aldrich),
459 penicillin–streptomycin (15140122, Thermo Fisher Scientific), GlutaMAX (35050061, Thermo Fisher
460 Scientific), MEM non-essential amino acids (11140035, Thermo Fisher Scientific), 1 mM sodium pyruvate
461 (11360070, Thermo Fisher Scientific) and 100 μM β-mercaptoethanol (31350-010, Thermo Fisher Scientific).
462 To maintain cells in pluripotency, 2i/LIF (1 mM MEK inhibitor PD0325901, 13034, Cayman Chemical; 3 mM
463 GSK3 inhibitor CHIR99021, 13122, Cayman Chemical; and 10 ng/ml leukemia inhibitory factor, LIF, A35933,
464 Gibco) was added to the Feeder Cell medium to preserve naïve pluripotency. N2B27 Medium: 1:1 mix of
465 DMEM F12 (21331-020, Thermo Fisher Scientific) and neurobasal A (10888-022, Thermo Fisher Scientific)
466 supplemented with 2% v/v B27 (10889-038, Thermo Fisher Scientific), 0.2% v/v N2 (17502048, Gibco),
467 100 μM β-mercaptoethanol (31350-010, Thermo Fisher Scientific), penicillin–streptomycin (15140122,
468 Thermo Fisher Scientific) and GlutaMAX (35050061, Thermo Fisher Scientific).

469

470 **Cell line list**

471

| Name | Description | Animal strains | Source | RRID | Reference |
|---|---|---|---|---|---|
| ES-E14 | Wildtype mouse embryonic stem cells | 129P2/Ola mice | Cambridge Stem Cell Institute | CVCL_C320 | (Hooper *et al*, 1987) |
| W4 | Wildtype mouse embryonic stem cells | 129S6/SvEvTacArc mice | Gifted from Shukry Habib at King's College London | CVCL_Y634 | (Auerbach *et al*, 2000) |
| *Cdh1* KO | E-cadherin knock-out mouse embryonic stem cells | 129S6/SvEvTacArc mice | Gifted from Lionel Larue at Institute Curie | | (Larue *et al*, 1996) |
| mCherry-PAR-6B ES-E14 | ES-E14 mouse embryonic stem cells expressing mCherry-PAR-6B | 129P2/Ola mice | Generated in this study | | |
| E-cadherin-eGFP ES-E14 | ES-E14 mouse embryonic stem cells expressing E-cadherin-eGFP | 129P2/Ola mice | Published in (Molè *et al*, 2021) | | (Molè *et al*, 2021) |
| LifeAct-mRuby ES-E14 | ES-E14 mouse embryonic stem cells expressing LifeAct-mRuby | 129P2/Ola mice | Generated in this study | | |
| LifeAct-mRuby *Cdh1* KO | E-cadherin knock-out mouse embryonic stem cells expressing LifeAct-mRuby | 129S6/SvEvTacArc mice | Generated in this study | | |

472

473

474 **siRNA transfection**

475 To achieve protein knockdowns, siRNA was transfected using Lipofectamine RNAiMAX according to the
476 manufacturer's instruction. mESCs cultured in 2D on the gelatin was transfected with 100 nM pre-designed
477 siRNA (s63752, Silencer Select). siRNA target mRNA sequences were: E-cadherin,
478 GAAGAUCACGUAUCGGAUU; P-cadherin, CGAAAGAGAGAGUGGGUGA; JAM-A,
479 GCCUUUGAUAGUGGUGAAU; Nectin-2, GGACUACUGAAUUCUUUUA. Two days after the first
480 transfection (Fig EV4A), the cells were cultured with or without mitomycin C and seeded into 10% Matrigel.
481 The cells were cultured in Matrigel with Lipofectamine RNAiMAX and 100 nM siRNA for another 24 hours,
482 then were subjected to further experiments and analysis.

483

## Immunofluorescence

Cells cultured in a µ-slide 8 well dish were fixed with 4% paraformaldehyde (J61899, Alfa Aesar) for 30 minutes at room temperature, then were permeabilised with 0.5% Triton X-100 for 15 minutes at room temperature. The cells were blocked with the incubation buffer (0.5% BSA, 0.1% Tween in PBS) for two hours, then were incubated with primary antibodies diluted in the incubation buffer at 4 □ overnight on shaking. The primary antibodies were washed off with PBS, then were incubated with secondary antibodies diluted in the incubation buffer at room temperature for two hours. The secondary antibodies were washed off with PBS. Samples cultured in Matrigel were kept in PBS; samples cultured in agarose were sealed in 200 µL 0.5% agarose. The samples were imaged shortly after. Antibodies and dilutions were as listed below.

## Antibody list

| **Primary antibodies** | | | | | |
|---|---|---|---|---|---|
| Protein | Catalog number | Supplier | Type | Specie | Concentrations |
| E-cadherin | ECCD-2 | Invitrogen | Monoclonal | Rat | 2 µg/mL |
| GM130 | 610822 | BD Biosciences | Monoclonal | Mouse | 1:300 |
| Nanog | ab80892 | Abcam | Polyclonal | Mouse | 1:300 |
| JAM-A | sc-52688 | Santa Cruz | Monoclonal | Rat | 1:300 |
| Nectin-2 | 502-57 | HycultBiotech | Monoclonal | Rat | 1:200 |
| OTX2 | AF1979 | R&D Systems | Polyclonal | Goat | 1:300 |
| PAR-3 | 07-330 | Merck Millipore | Polyclonal | Rabbit | 1:100 |
| P-cadherin | AF761 | R&D Systems | Polyclonal | Goat | 1:500 |
| Podocalyxin | MAB1556 | R&D Systems | Monoclonal | Rat | 3.3 µg/mL |
| Γ-Tubulin | T6557 | Sigma-Aldrich | Monoclonal | Mouse | 1:250 |
| ZO-1 | 61-7300 | Invitrogen | Polyclonal | Rabbit | 1:500 |

| **Secondary antibodies** | | | |
|---|---|---|---|
| Name | Supplier | Target/Catalog number | Concentrations |
| Alexa Fluor 488 | Invitrogen | Rat | 1:500 |
| Alexa Fluor 488 | Invitrogen | Rabbit | 1:500 |
| Alexa Fluor 488 | Invitrogen | Goat | 1:500 |
| Alexa Fluor 546 | Invitrogen | Mouse | 1:500 |
| Alexa Fluor 555 | Invitrogen | Goat | 1:500 |
| DyLight 550 | Invitrogen | Rat | 1:500 |
| CF 633 | Insight Biotech | Phalloidin | 6.6 pM |
| 4′,6-diamidino-2-phenylindole, DAPI | Sigma | D8417 | 0.5 µg/mL |

## Microscope imaging

Live cell imaging was carried out on the PerkinElmer UltraVIEW spinning disk system fitted on an Olympus IX80 confocal microscope with a 37 □ and 5% $CO_2$ chamber. Images were captured with the 40x 1.3 NA (oil) objective, 2x Hamamatsu Orca-R2 CCD camera and Volocity 3.7.1 software. The cells were imaged at 2 µm z-step size and 30 minutes time intervals. Fixed samples were imaged on the Leica SP8 confocal microscope with the 40x 1.3 NA (oil) or 63x 1.4 NA (oil) objective and LAS X 3.7.4 software. The cells were imaged at 0.3 µm z-step size and 2X line average. FRAP was performed on the Zeiss LSM-900 confocal

microscope with 63X, 1.40NA Plan Apo objective and ZEN Blue 2.1 software equipped with a 37 °C heated stage.

**Image and data analysis**

The central section images were projected from raw images in the Fiji software by maximum-value projection of the whole z stacks to produce the 3D projection images, or of the central three image of the z stacks to produce the central-section images. The whole z stacks projections were applied to count cell cluster percentages. The central-section images were applied for line-scans or analysis of region of interest to determine protein signals.

The mESCs with positive or negative protein centres were manually determined and counted. The percentage was calculated with the number relative to the number of total cell clusters captured in each condition. The mean percentages from three independent experiments were compared with student's t-test or one-way ANOVA specified in figure legends using the GraphPad Prism software. Sample sizes are specified in figure legends.

To quantify PAR-3 signal along the cell-cell interface, a 0.8μm width line was drawn alone the cell-cell interface by using F-actin (labelled by Phalloidin) or E-cadherin signal as the path. PAR-3 and F-actin pixel values along the path were extracted. The two peaks of F-actin signals at two ends of the path were determined as the start and end of the cell-cell interface and the positions in-between were defined as 1X cell-cell interface. The corresponding PAR-3 pixel to the F-actin peak positions were identified and the PAR-3 line-profile between the two positions were sectioned to 20 sections. PAR-3 pixel value in each section was averaged to be the PAR-3 signal in 5% of the cell-cell interface. The values from 10-20 cells were plotted as line graphs.

To compare the level of PAR-3 at the centre and outer regions in multi-cell mESC clusters, a 4 μm diameter circular area was created in the Fiji software and placed over the multi-cellular joint in a cell cluster, and the average PAR-3 fluorescence values in the circle was measured. The boundary of the cell cluster was drawn by the free-hand tool in Fiji by using the correspondent F-actin signal, and the average PAR-3 fluorescence values between the circle and the boundary were measured. The ratio between the PAR-3 values in the circle and outer regions was then calculated.

To generate the PAR-3 signal heatmap, based on the F-actin signal, a squared region of interest was created in the Fiji software for every cell, which the main cell body of a cell was fitted into. The PAR-3 image in each squared region was transformed into a 10 x 10-unit matrix by using the R-language. Each unit was created by averaging the PAR-3 fluorescence intensity in every 10% length along the X or Y axis of the squared region of interest extracted from the original image. A serial of images from one condition of an experiment was stacked and the averaged pixel value at each position was calculated to generate an averaged 10 x 10 matrix. The final matrix was transformed into a heatmap in the GraphPad Prism software.

To compare the level of PAR-3 in the core areas in the cells culture on the glass, a 6 μm diameter circular area of interest was created in the Fiji software to cover the PAR-3 core area in a cell, and the average PAR-3 fluorescence values in the circle was measured. The boundary of the cell was drawn by the free-hand tool in Fiji, and the average PAR-3 fluorescence values in the boundary was measured. The ratio between the PAR-3 values in the circle and inside the boundary was then calculated.

Sample sizes and statistical analysis are detailed in the figure legends. No blinding was done for the experiments in this study. Instead, we included direct continuous measurements (e.g. of fluorescent intensity) alongside categorical analyses. To assess AMIS localisation independently to cell division, we did not include control cells that were undergoing mitosis (identified by chromosome and cell morphologies) into the quantifications. We checked that excluding this data made no difference to the outcome of the analyses.

**FRAP**

FRAP of E-cadherin-eGFP was performed to measure E-cadherin dynamics at the cell-cell interface. A E-cadherin-eGFP expressing stable ES-E14 line was used to perform the experiment (Molè *et al*, 2021). After 24 hours culturing in Matrigel, two-cell clusters with long axis parallel to surface of the culture dish, hence the cell-cell interfaces were aligned to the axis of the objective were used for FRAP. A region of interest (ROI) of 2 X 1 μm along xy-axis was chosen at the approximately centre-most region or side regions at each cell-cell interface. The ROI in a series of z-axis stacks with 0.3 μm intervals cross 2 μm was bleached with 3 iterations of the 488 nm laser with 100% transmission. This resulted in a photobleaching of over 80% in a 2 X 2 μm (xz-axis) region at the cell-cell interface. Time-lapse images were acquired before (3 frames) and after (30 frames) photobleaching with an interval of 10s per frame. Average fluorescence intensity values $F(t)$ in the bleached area within the centre z-stack were analysed with ImageJ. The mean values of the three frames before bleaching was used as the pre-bleached value $F(i)$. The value of the first frame after bleaching was defined as $F(0)$. FRAP values were then calculated and plotted over time in Fig 3J as:

$$\mathrm{FRAP} = \frac{F(t) - F(0)}{F(i) - F(0)}$$

The FRAP values were fitted using a non-linear regression and the exponential one-phase association model using Y0 = 0 and where mobile fraction corresponds to the plateau value in the GraphPad Prism software. For Fig 3K, the mobile fraction from each FRAP profile was pooled and compared between conditions.

**Data and code availability**

Image data is accessible in the BioImage Archive, accession number S-BIAD473.
The R-language code for generating the PAR-3 heatmap in Figure 5D is accessible at:
https://github.com/Buckley-Lab-opto/Liang-2022

**Acknowledgements**

We are grateful to Jon Clarke and Ben Steventon for critical reading of the manuscript and other members of the Buckley and Zernicka-Goetz labs for scientific discussion, especially Matteo Molè and Marta Shahbazi. Thank you to the Shukry Habib lab for kindly gifting the W4 cells and the Lionel Larue lab for kindly gifting the *Cdh1* KO cells. Thank you to the Cambridge Advanced Imaging Centre and the Ewa Paluch lab for help and access to confocal microscopy.

Funding: This research was financially supported by: CEB - the Wellcome Trust and Royal Society (Sir Henry Dale Fellowship grant no. 208758/Z/17/Z and Dorothy Hodgkin Fellowship grant no. DH160086), XL - European Union's Horizon 2020 programme (Marie Skłodowska-Curie Individual Fellowship grant no. 844330), the Issac Newton Trust and Leverhulme Trust (Leverhulme Early Career Fellowship grant no. ECF-2019-175). MZG - The Wellcome Trust (207415/Z/17/Z) and ERC (669198). For the purpose of open access, the authors have applied a Creative Commons Attribution (CC BY) licence to any Author Accepted Manuscript version arising.

## Author contributions

Conceptualisation: CEB, XL. Methodology: XL, CEB, AW. Formal analysis: XL, CYH. Investigation: XL, AW. Writing: CEB, XL. Visualisation: XL. Supervision: CEB, MZG. Funding acquisition: CEB, XL, MZG.

## Conflict of interest

The authors declare that they have no conflict of interest.

## References

Akhtar N & Streuli CH (2013) An integrin--ILK--microtubule network orients cell polarity and lumen formation in glandular epithelium. *Nat Cell Biol* 15: 17–27

Auerbach W, Dunmore JH, Fairchild-Huntress V, Fang Q, Auerbach AB, Huszar D & Joyner AL (2000) Establishment and Chimera Analysis of 129/SvEv- and C57BL/6-Derived Mouse Embryonic Stem Cell Lines. *Biotechniques* 29: 1024–1032

Bedzhov I & Zernicka-Goetz M (2014) Self-organizing properties of mouse pluripotent cells initiate morphogenesis upon implantation. *Cell* 156: 1032–44

Blasky AJ, Mangan A & Prekeris R (2015) Polarized protein transport and lumen formation during epithelial tissue morphogenesis. *Annu Rev Cell Dev Biol* 31: 575–591

Bryant DM, Datta A, Rodriguez-Fraticelli AE, Peranen J, Martin-Belmonte F & Mostov KE (2010) A molecular network for de novo generation of the apical surface and lumen. *Nat Cell Biol* 12: 1035–1045

Bryant DM, Roignot J, Datta A, Overeem AW, Kim M, Yu W, Peng X, Eastburn DJ, Ewald AJ, Werb Z, *et al* (2014) A molecular switch for the orientation of epithelial cell polarization. *Dev Cell* 31: 171–187

Buckley CE & Johnston DS (2022) Apical–basal polarity and the control of epithelial form and function. *Nat Rev Mol Cell Bio*: 1–19

Buckley CE, Ren X, Ward LC, Girdler GC, Araya C, Green MJ, Clark BS, Link BA & Clarke JDW (2013) Mirror-symmetric microtubule assembly and cell interactions drive lumen formation in the zebrafish neural rod. *Embo J* 32: 30–44

Ciruna B, Jenny A, Lee D, Mlodzik M & Schier AF (2006) Planar cell polarity signalling couples cell division and morphogenesis during neurulation. *Nature* 439: 220–224

Ebnet K, Suzuki A, Horikoshi Y, Hirose T, Brickwedde MKMZ, Ohno S & Vestweber D (2001) The cell polarity protein ASIP/PAR-3 directly associates with junctional adhesion molecule (JAM). *Embo J* 20: 3738–3748

Herrera A, Menendez A, Torroba B, Ochoa A & Pons S (2021) Dbnl and β-catenin promote pro-N-cadherin processing to maintain apico-basal polarity. *J Cell Biol* 220: e202007055

Hooper M, Hardy K, Handyside A, Hunter S & Monk M (1987) HPRT-deficient (Lesch–Nyhan) mouse embryos derived from germline colonization by cultured cells. *Nature* 326: 292–295

Iden S, Rehder D, August B, Suzuki A, Wolburg-Buchholz K, Wolburg H, Ohno S, Behrens J, Vestweber D & Ebnet K (2006) A distinct PAR complex associates physically with VE-cadherin in vertebrate endothelial cells. *Embo Rep* 7: 1239–1246

Ishida S, Tanaka R, Yamaguchi N, Ogata G, Mizutani T, Kawabata K & Haga H (2014) Epithelial Sheet Folding Induces Lumen Formation by Madin-Darby Canine Kidney Cells in a Collagen Gel. *Plos One* 9: e99655

Itoh M, Sasaki H, Furuse M, Ozaki H, Kita T & Tsukita S (2001) Junctional adhesion molecule (JAM) binds to PAR-3: a possible mechanism for the recruitment of PAR-3 to tight junctions. *J Cell Biology* 154: 491–7

Jia L, Liu F, Hansen SH, Beest MBA ter & Zegers MMP (2011) Distinct roles of cadherin-6 and E-cadherin in tubulogenesis and lumen formation. *Mol Biol Cell* 22: 2031–2041

Kim YS, Fan R, Kremer L, Kuempel-Rink N, Mildner K, Zeuschner D, Hekking L, Stehling M & Bedzhov I (2021) Deciphering epiblast lumenogenesis reveals proamniotic cavity control of embryo growth and patterning. *Sci Adv* 7: eabe1640

Klinkert K, Rocancourt M, Houdusse A & Echard A (2016) Rab35 GTPase couples cell division with initiation of epithelial apico-basal polarity and lumen opening. *Nat Commun* 7: 11166

Larue L, Antos C, Butz S, Huber O, Delmas V, Dominis M & Kemler R (1996) A role for cadherins in tissue formation. *Development* 122: 3185–3194

Li D, Mangan A, Cicchini L, Margolis B & Prekeris R (2014) FIP5 phosphorylation during mitosis regulates apical trafficking and lumenogenesis. *Embo Rep* 15: 428–37

Luján P, Varsano G, Rubio T, Hennrich ML, Sachsenheimer T, Gálvez-Santisteban M, Martín-Belmonte F, Gavin A-C, Brügger B & Köhn M (2016) PRL-3 disrupts epithelial architecture by altering the post-mitotic midbody position. *J Cell Sci* 129: 4130–4142

Mangan AJ, Sietsema DV, Li D, Moore JK, Citi S & Prekeris R (2016) Cingulin and actin mediate midbody-dependent apical lumen formation during polarization of epithelial cells. *Nat Commun* 7: 12426

Molè MA, Weberling A, Fässler R, Campbell A, Fishel S & Zernicka-Goetz M (2021) Integrin β1 coordinates survival and morphogenesis of the embryonic lineage upon implantation and pluripotency transition. *Cell Reports* 34: 108834

Morais-de-Sa E, Mirouse V & Johnston DS (2010) aPKC phosphorylation of Bazooka defines the apical/lateral border in Drosophila epithelial cells. *Cell* 141: 509–23

Nikolopoulou E, Galea GL, Rolo A, Greene NDE & Copp AJ (2017) Neural tube closure: cellular, molecular and biomechanical mechanisms. *Development* 144: 552–566

668 Noordstra I, Hermoso MD, Schimmel L, Bonfim-Melo A, Kalappurakkal JM, Mayor S, Gordon E, Cusachs PR & Yap
669 AS (2021) Cortical actin flow activates an α-catenin clutch to assemble adherens junctions. *Biorxiv*:
670 2021.07.28.454239

671 Quesada-Hernandez E, Caneparo L, Schneider S, Winkler S, Liebling M, Fraser SE & Heisenberg CP (2010)
672 Stereotypical Cell Division Orientation Controls Neural Rod Midline Formation in Zebrafish. *Curr Biol* 20: 1966–
673 72

674 Rathbun LI, Colicino EG, Manikas J, O'Connell J, Krishnan N, Reilly NS, Coyne S, Erdemci-Tandogan G, Garrastegui
675 A, Freshour J, *et al* (2020) Cytokinetic bridge triggers de novo lumen formation in vivo. *Nat Commun* 11: 1269

676 Schlüter MA, Pfarr CS, Pieczynski J, Whiteman EL, Hurd TW, Fan S, Liu C-J & Margolis B (2009) Trafficking of
677 Crumbs3 during cytokinesis is crucial for lumen formation. *Mol Biol Cell* 20: 4652–4663

678 Shahbazi MN, Scialdone A, Skorupska N, Weberling A, Recher G, Zhu M, Jedrusik A, Devito LG, Noli L, Macaulay
679 IC, *et al* (2017) Pluripotent state transitions coordinate morphogenesis in mouse and human embryos. *Nature* 552:
680 239–243

681 Soncin F, Mohamet L, Eckardt D, Ritson S, Eastham AM, Bobola N, Russell A, Davies S, Kemler R, Merry CLR, *et al*
682 (2009) Abrogation of E-Cadherin-Mediated Cell–Cell Contact in Mouse Embryonic Stem Cells Results in
683 Reversible LIF-Independent Self-Renewal. *Stem Cells* 27: 2069–2080

684 Symonds AC, Buckley CE, Williams CA & Clarke JDW (2020) Coordinated assembly and release of adhesions builds
685 apical junctional belts during de novo polarisation of an epithelial tube. *Development* 147: dev191494

686 Takekuni K, Ikeda W, Fujito T, Morimoto K, Takeuchi M, Monden M & Takai Y (2003) Direct Binding of Cell
687 Polarity Protein PAR-3 to Cell-Cell Adhesion Molecule Nectin at Neuroepithelial Cells of Developing Mouse*. *J*
688 *Biol Chem* 278: 5497–5500

689 Tawk M, Araya C, Lyons DA, Reugels AM, Girdler GC, Bayley PR, Hyde DR, Tada M & Clarke JD (2007) A mirror-
690 symmetric cell division that orchestrates neuroepithelial morphogenesis. *Nature* 446: 797–800

691 Thomas FC, Sheth B, Eckert JJ, Bazzoni G, Dejana E & Fleming TP (2004) Contribution of JAM-1 to epithelial
692 differentiation and tight-junction biogenesis in the mouse preimplantation embryo. *J Cell Sci* 117: 5599–5608

693 Wang L-T, Rajah A, Brown CM & McCaffrey L (2021) CD13 orients the apical-basal polarity axis necessary for lumen
694 formation. *Nat Commun* 12: 4697

695 Wang T, Yanger K, Stanger BZ, Cassio D & Bi E (2014) Cytokinesis defines a spatial landmark for hepatocyte
696 polarization and apical lumen formation. *J Cell Sci* 127: 2483–92

697 Yu W, Datta A, Leroy P, O'Brien LE, Mak G, Jou T-S, Matlin KS, Mostov KE & Zegers MMP (2004) Beta1-integrin
698 orients epithelial polarity via Rac1 and laminin. *Mol Biol Cell* 16: 433–45

699 Zhang Y, Mets RD, Monzel C, Acharya V, Toh P, Chin JFL, Hul NV, Ng IC, Yu H, Ng SS, *et al* (2020) Biomimetic
700 niches reveal the minimal cues to trigger apical lumen formation in single hepatocytes. *Nat Mater* 19: 1026–1035

701 Zigman M, le AT, Fraser SE & Moens CB (2011) Zebrafish neural tube morphogenesis requires scribble-dependent
702 oriented cell divisions. *Curr Biol* 21: 79–86

703

704

## Figure Legends

**Figure 1 - Cell division is dispensable for AMIS localisation in mESC 3D cultures in Matrigel.**

A Stages of polarisation and lumen formation in mESCs cultured in Matrigel.

B Timeline of experiment setups to assess AMIS formation.

C Immunofluorescence of PAR-3 and E-cadherin. PAR-3 localisation was concentrated at the centre of 2-cell mESC doublets and 3- or 4-cell mESC clusters, whilst E-cadherin was localised along the whole length of cell-cell interfaces in both control and mitomycin C treated conditions.

D Quantification of the frequency of cell clusters with a strong polarised PAR-3 centre. See the representative mESC clusters without the strong polarised PAR-3 in Appendix Fig S1A,B.

E Illustrations of PAR-3 analysis in 2-cell (a) and >2-cell (b) clusters. The line-scan analysis was performed from the yellow arrow to the orange arrow at the cell-cell interface between two cells in (a). The average pixel intensity was analysed at central (red region, inner dotted line) and surrounding non-central regions (orange region, between the inner and outer dotted lines) in (b).

F Line-scan profiles of PAR-3 at the cell-cell interface of 2-cell mESC doublets. Line scans were sectioned and fitted to each 5% along the cell-cell interface length.

G Ratio of PAR-3 pixel intensity values at central and surrounding regions in >2-cell mESC clusters.

H, I Representative images of centralised ZO-1 puncta and polarised Golgi apparatus, labelled by GM130 (H) and quantification of the frequency of cell doublets with a polarised ZO-1 or Golgi apparatus centre (I). Also see the spilt channels in Appendix Fig S1C.

J, K Representative images of polarised centrosomes (J), labelled with γ-tubulin and distance between centrosomes (K) normalised to the length of the long axis of the doublets in 2-cell clusters.

Data information: Data are presented as means ± SEM in (D) & (I); individual line-scans and mean valued line-scans in (F); individual cell cluster values (small dots), mean experimental values (large dots) and means of 3 experiments (bars) in (G); individual values in dots and median values in bars in (K). n = 3 experiments in (D) & (I), 15-32 cell clusters were analysed for each column in every experiment; 15 cell doublets for each condition from one experiment in (F); 15-22 cell clusters for each condition in every experiment in (G); 35 doublets for each condition in (K). Two-way ANOVA analysis in (D); student's t-test analysis in (G), (I), (K). *P* values were listed in the graphs. All scale bars: 10 μm.

**Figure 2 - Polarised PAR6B in mESC 3D cultures.**

A Representative images of mCherry-PAR-6B mESC live cells cultured from 24 – 96 hours in Matrigel. See the bight-filed images in Fig S2A.

B, C Representative images (B) and quantification of the frequency of cell clusters with polarised mCherry-PAR-6B (C) in control and mitomycin division-blocked mESC live cells after 24 hours in Matrigel.

D Movie stills of mCherry-PAR-6B in control and mitomycin C treated mESCs cultured in Matrigel (also Movie EV2). Control cells divided (i) and two mitomycin treated cells touched (ii) to form 2-cell doublets. Control cells divided twice (iii) and two mitomycin treated cell clusters touched (iv) to form 4-cell clusters. (v), Kymograph of mCherry-PAR6B in the arrow-head cell in (ii) along the path between the arrows; each pixel is the fluorescence values averaged over 0.2 μm sections. See more examples in Appendix Fig S2D,E.

Data information: Data in (C) are presented as means ± SEM. n = 3 experiments. At least 20 clusters were analysed for each column in every experiment. Two-way ANOVA analysis; *P* values were listed in the graphs. All scale bars: 10 μm.

**Figure 3 - E-cadherin junctions are important for polarisation.**

A, B Immunofluorescence of PAR-3 (A) and proportions of mESC clusters with a strong PAR-3 centre (B) in wild-type (W4) and E-cadherin knock-out (*Cdh1* KO) mESCs at 24 hrs in Matrigel. See E-cadherin in Appendix Fig S3A.

C Line-scan profiles of PAR-3 at the cell-cell interface in wild-type control, mitomycin C treated and *Cdh1* KO control, mitomycin C treated 2-cell doublets.

D Ratio of PAR-3 pixel intensity values at central and surrounding regions in >2-cell mESC clusters.

E, F Representative images of PAR-3 immunofluorescence (E) and line-scan profiles of PAR-3 at the cell-cell interface (F) in WT homogeneous or WT (ES-E14) /*Cdh1* KO chimeric mESC 2-cell doublets. *, WT mESCs.

G, H Representative images of ZO-1 puncta and Golgi apparatus (G) and proportions of mESC doublets with central ZO-1 puncta or polarised Golgi apparatus (H) in WT and *Cdh1* KO mESC doublets.

I Distance between centrosomes in cell doublets. The distance was normalised to the length of the long axis of the doubles. See the representative images in Appendix Fig S3D.

J Fluorescence recovery after photobleaching (FRAP) of E-cadherin-eGFP at the centre-most or side 2 μm regions of division-blocked mESC doublets' cell-cell interfaces. See methods in Fig EV2C.

K Mobile fraction of E-cadherin-eGFP calculated from the plotting of (J).

Data information: Data are presented as means ± SEM in (B), (H); individual and mean-valued line-scans in (C) & (F); individual cell cluster values (small dots), mean experimental values (large dots) and means of 3 experiments (bars) ± SEM in (D); individual values in dots and median values in bars in (I); exponential association fitting curves ± SD in (J); means ± SD in (K). n = 3 experiments in (B) & (H), 17-50 cell clusters were analysed for each column in every experiment; 15 doublets for each condition in (C); 17-30 cell clusters were analysed for each condition in every experiment in (D); 15 doublets for each condition in (F); 35-40 doublets in each condition in (I); 15-18 doublets for each condition in (J) & (K). Two-way ANOVA analysis in (B), (D), (I) & (K); student's t-test analysis in (H); *P* values were listed in the graphs. All scale bars: 10 μm.

**Figure 4 - Adhesion molecule P-cadherin, JAM-A and Nectin-2 do not aid PAR-3 in the AMI**S.

A-C Immunofluorescence of PAR-3 and P-cadherin (A), proportions of mESC clusters with a positive PAR-3 centre (B) and line-scans of PAR-3 at the cell-cell interface (C) in control, P-cadherin knock-down by RNAi, mitomycin treated and P-cadherin knock-down mitomycin treated W4 mESC doublets cultured for 24 hours in Matrigel.

D-F Immunofluorescence of PAR-3 and JAM-A (D), proportions of mESC clusters with a positive PAR-3 centre (E) and line-scans of PAR-3 at the cell-cell interface (F) in control, JAM-A knock-down by RNAi, mitomycin treated and JAM-A knock-down mitomycin treated W4 mESC doublets cultured for 24 hours in Matrigel.

G-I Immunofluorescence of PAR-3 and Nectin-2 (G), proportions of mESC clusters with a positive PAR-3 centre (H) and line-scans of PAR-3 at the cell-cell interface (I) in control, Nectin-2 knock-down by RNAi, mitomycin treated and Nectin-2 knock-down mitomycin treated W4 mESC doublets cultured for 24 hours in Matrigel.

Data information: Data are presented as means ± SEM in (B), (E), (H); individual and mean-valued line-scans in (C), (F), (I). n = 3 experiments in (B), (E), (H), 15-21 clusters were analysed for each column in every experiment; 15-21 line-scans in (C), (F), (I). Two-way ANOVA analysis in (B), (E), (H); *P* values were listed in the graphs. All scale bars: 5 μm.

**Figure 5 - Cell-ECM interactions in regulating AMIS seeding.**

A, B Immunofluorescence of PAR-3 (A) and proportions of mESC doublets with polarised PAR-3 (B) in wild-type (ES-E14) and E-cadherin knock-out (*Cdh1* KO) cells at 30 hours in 0.5% agarose.

C Immunofluorescence of PAR-3 in cell division blocked mESCs cultured on E-cadherin or Fibronectin coated glass topped with or without Matrigel for 24 hours.

D Heatmap of PAR-3 in cells from one experiment of (C). Squared frames were fitted to the main bodies of the cells. A pixel was the average value in each 10% along the width of the frames. The heatmaps were stacks of 15 cells in one experiment.

E PAR-3 levels at the central 20% of the heatmaps from three experiments of (C).

F Ratios between PAR-3 in the 2.5 μm diameter central core and whole cell surface from three experiments of (C).

Data information: Data are presented as means ± SEM in (B); individual cell values (small dots), mean experimental values (large dots) and means of experiments ± SEM (bars) in (E) & (F). n = 3 experiments in (B), (E), (F); at least 15 clusters were analysed for each column in every experiment; 15 - 20 cells for each column in every experiment of (E) & (F). Two-way ANOVA analysis in (B), (E), (F); *P* values were listed in the graphs. All scale bars: 5 μm.

**Figure 6 - Lumenogenesis in wild-type and E-cadherin knock-out mESC cultures.**

A PAR-3 immunofluorescence in wild-type (ES-E14) and E-cadherin knock-out (*Cdh1* KO) mESCs cultured in Matrigel for 48 and 72 hours. At 48 hours, most WT cell clusters had formed a polarised rosette or small lumen (i). However, most Cdh1 KO cells had not formed a central AMIS (ii). A small percentage of Cdh1 KO cells had formed an open ‘cup-shape’, with apically localised PAR-3 (iii). By 72 hours, a significant proportion of Cdh1 KO cells had formed polarised ‘cavity-like’ structures, about half of which were configured in an open ‘cup-shape’ and half as closed ‘lumen-like’ structures (iv).

B Podocalyxin immunofluorescence in WT and Cdh1 KO mESCs cultured in Matrigel from 1-4 days. See Fig EV5A for ZO-1 staining.

C Examples of masked *Cdh1* KO cell cluster surfaces from ‘open’ and ‘closed’ cavities. The cavities were categorised based on Podocalyxin signals.

D Percentage of cell clusters with different cavities relative to total cell clusters at different time points. The analysis was compared between the closed/rosette category among the conditions.

E Percentage of cell clusters with closed cavities relative to total cell clusters with cavities calculated from (D).

F Movies stills of LifeAct-mRuby labelled cell clusters. The images are whole cell cluster z-projections, overlaid with 3D rendering of the cluster surfaces to show the forming lumens. See Movie EV3 for z-stack movies and Movie EV4 for 3D rotations.

Data information: Data are presented as means ± SEM in (D) & (E). n = 20 (48 hours WT & *Cdh1* KO), 30 (72 hours WT) and 32 (72 hours *Cdh1* KO) images in (A); 3 experiments in (D) & (E), at least 25 clusters were analysed for each column in every experiment. Two-way ANOVA analysis in (D) & (E); *P* values were listed in the graphs. All scale bars: 25 μm.

**Figure 7 - Synopsis of *de novo* polarisation and lumenogenesis.**

A *De novo* polarisation and AMIS formation in dividing and division-blocked mESCs cultured in Matrigel.

B Lumenogenesis in wide-type and E-cadherin knock-out mESCs cultured in Matrigel.

## Extended Viewer Figure and Movies legends

### Figure EV1 - Division blocked mESCs in Matrigel 3D cultures.

A Percentage of cells that divided or did not divide in control cells or following mitomycin C treatment. Cell numbers were taken from live movies of the first 24 hours following seeing into Matrigel. Mitomycin C sufficiently blocked cell divisions.

B Movie stills of mitomycin C treated cells from Movie EV1.

C Quantification of E-cadherin fluorescence intensity at cell-cell interfaces and cell-matrix interfaces in 2-cell mESC clusters.

D Percentage of cells that divided or did not divide in control cells or following aphidicolin treatment. Cell numbers were taken from live movies of the first 24 hours following seeing into Matrigel. Aphidicolin sufficiently blocked cells divisions.

E, F Immunofluorescence of PAR-3 (E) and percentages of 2-cell mESC clusters with a positive PAR-3 centre (F) in control and aphidicolin treated cells cultured for 24 hours in Matrigel.

G, H Immunofluorescence of ZO-1 and Golgi apparatus (G) and percentages of 2-cell mESC clusters with a strong positive ZO-1 centre or polarised Golgi apparatus (H) in control and aphidicolin treated cells.

Data information: All data are presented as means ± SEM. n = total numbers of cells tracked at time point zero in (A) & (D); 18 cell clusters in each condition in (C); 3 experiments in (F), (H), 20 clusters were analysed for each column in every experiment. Student's t-test analysis in (C) and (H); two-way ANOVA analysis in (F); *P* values were listed in the graphs. All scale bars: 10 μm.

### Figure EV2 - E-cadherin in the centre-most and side regions at two-cell cluster interfaces.

A An example line-scan at the centre-most (blue) and side (red) regions at division blocked two-cell cluster interfaces. The width of line-scans was 3 μm. Two side regions were line-scanned, and the average was taken as the line-scan profile at the side regions for a two-cell cluster (See panel B).

B Line-scan profiles of E-cadherin at the centre-most and side regions. The statistical comparison was done between the area under the curves.

C Illustrations of E-cadherin-eGFP FRAP at a two-cell cluster interface.

D Average E-cadherin-eGFP pixel levels at the photo bleaching regions before bleaching in division blocked cells.

Data information: In (B) & (D), data are means ± SD; n = 15 cell clusters; student's t-test analysis; *P* values were listed in the graphs.

**Figure EV3 - AMIS seeding and pluripotency exit in wild-type and E-cadherin knock-out mESCs.**

A Timeline of experiment setups to assess *de novo* polarisation when mESCs were cultured with 2i/LIF to remain pluripotent.

B, C Immunofluorescence of PAR-3 (B) and quantification of the proportion of cell clusters with a polarised PAR-3 centre (C) in wild-type (ES-E14) and *Cdh1* knock-out (KO) mESCs cultured in Matrigel for 24 hours with 2i/LIF.

D Nuclear levels of OTX2 and NANOG based on immunofluorescence in wild-type and *Cdh1* KO mESCs at 12 or 24 hours post seeding into Matrigel. Only cells in interphase were analysed.

Data information: Data are presented as means ± SEM in (C); values of individual cells in dots and means ± SD in bars in (D). n = 3 experiments in (C), at least 20 clusters were analysed for each column in every experiment; 17-45 cells in each column from one experiment in (D). Two-way ANOVA analysis in (C) & (D); *P* values were listed in the graphs. Scale bar: 10 μm.

**Figure EV4 - Expression and knock-down of P-cadherin, JAM-A and Nectin-2 in mESCs.**

A Expression and knock-down of E-cadherin, P-cadherin, JAM-A and Nectin-2 in mESCs (W4) cultured in 2D on gelatin. Scale bar: 15 μm.

B-D Expression of PAR-3 and P-cadherin (B), JAM-A (C) and Nectin-2 (D) in control and knock-down 4-cell mESC clusters cultured 24 hours in Matrigel. Scale bars: 15 μm.

E-G Expression of PAR-3 and P-cadherin (E), JAM-A (F) and Nectin-2 (G) in wild-type (W4) and E-cadherin knock-out (KO) mESC clusters cultured 24 hours in Matrigel. Scale bars: 15 μm.

**Figure EV5 - Wild-type and E-cadherin knock-out mESC cultured in Matrigel during lumenogenesis.**

A ZO-1 immunofluorescence in wild-type (ES-E14) and E-cadherin knock-out (*Cdh1* KO) mESCs cultured in Matrigel from 1-4 days. See Fig 6B for Podocalyxin staining. Scale bars: 25 μm.

B The Golgi network, phospho-myosin light chain 2 and F-actin in *Cdh1* KO mESCs cultured for 72 hours in Matrigel. Scale bars: 25 μm.

**Movie EV1 - Bright-field live movies of control and mitomycin-treated mESCs cultured in Matrigel.**

A, B Control mESCs cultured in Matrigel from 0 – 24 hours divided one (A) or two times (B).

C, D Mitomycin C treated mESC cultured in Matrigel from 0 – 24 hours did not divide but formed 2-cell clusters (C) or >2-cell clusters (D). Scale bar: 10 μm.

**Movie EV2 - Representative movies of mCherry-PAR6B in dividing and division-blocked mESCs cultured in Matrigel.**

A, B Control (A) and mitomycin division-blocked (B) mESCs cultured in Matrigel formed 2-cell doublets from 6 – 18 hours in Matrigel.

C, D Control (C) and mitomycin division-blocked (D) mESCs cultured in Matrigel formed multi-cell clusters from 9 – 19 hours in Matrigel. mCherry-PAR-6B localised to cell-cell contacts between 2 cells or the centre of multi-cell clusters after cell divisions (A, C) or after the cells touched (B, D). Scale bar: 10 μm.

**Movie EV3 - Representative movies of cysts forming in wild-type and E-cadherin knock-out mESCs cultured in Matrigel.**

Representative movies of the central 5μm z-stack of LifeAct-mRuby mESCs from control and cdh1 KO cell clusters as they make lumens.

A Wild-type mESCs cultured from 48 – 69 hours, frame interval = 1 hour.

B Cdh1 KO mESCs cultured from 48 – 68 hours, frame interval = 1 hour.

C Wild-type mESCs cultured from 74 – 83.5 hours, frame interval = 1 hour.

D Cdh1 KO mESCs cultured from 78 – 88.5 hours, frame interval = 30 min.

Scale bars: 25 μm.

**Movie EV4 - Rotation of the 3D rendering in Figure 6F.**

3D Rendering of wide-type (A) and E-cadherin knock-out (*Cdh1* KO, B) mESCs cultured in Matrigel. Central 5 μm of mESC cultures is shown at the end of the movie to better see the forming lumens. Scale bars: 10 μm.

1011

**Figure 1**

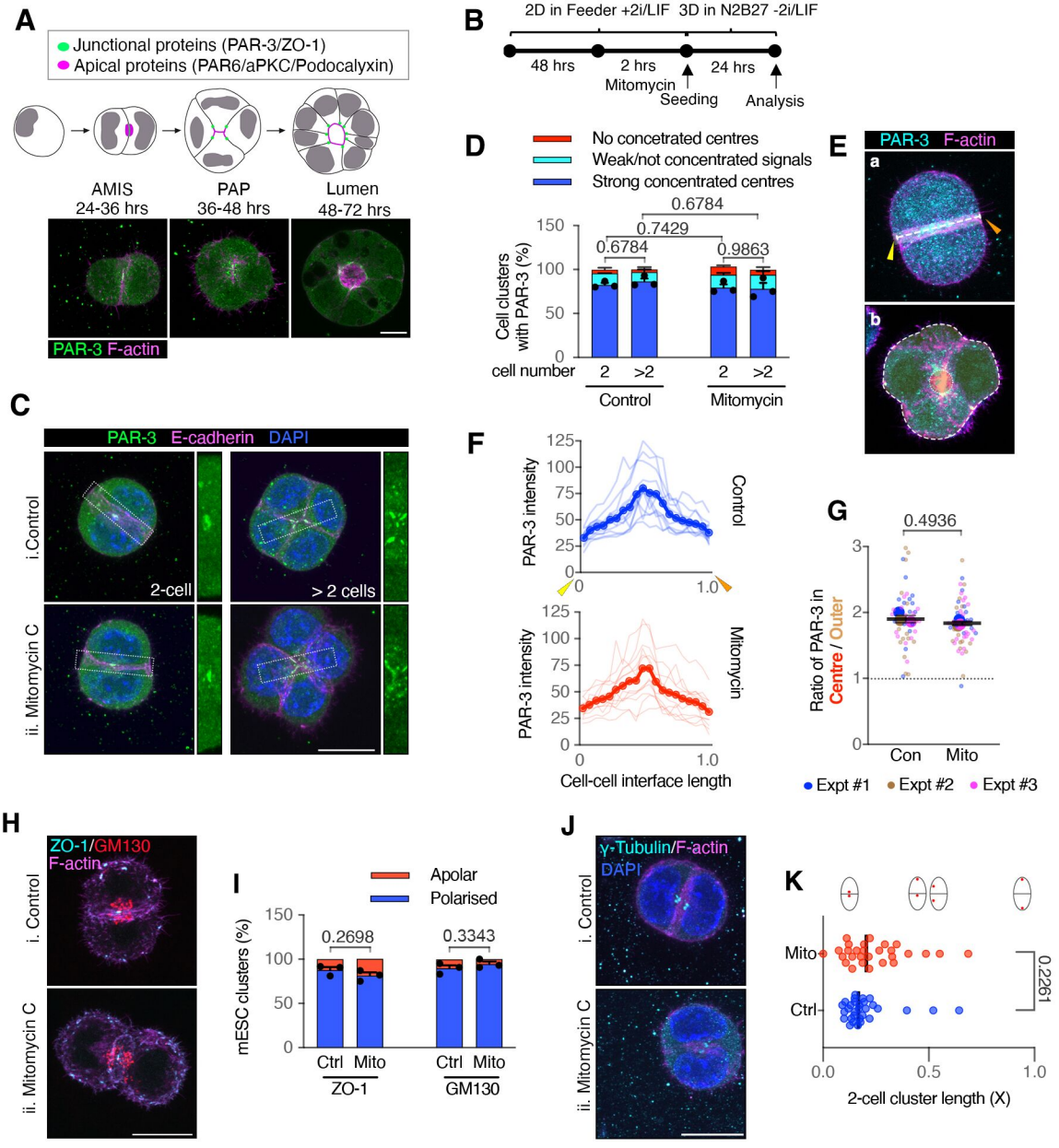
A
Junctional proteins (PAR-3/ZO-1)
Apical proteins (PAR6/aPKC/Podocalyxin)
AMIS
24-36 hrs
PAP
36-48 hrs
Lumen
48-72 hrs
PAR-3 F-actin
B
2D in Feeder +2i/LIF
3D in N2B27 -2i/LIF
48 hrs
2 hrs
Mitomycin
24 hrs
Seeding
Analysis
C
PAR-3 E-cadherin DAPI
i.Control
ii. Mitomycin C
2-cell
> 2 cells
D
No concetrated centres
Weak/not concentrated signals
Strong concentrated centres
Cell clusters with PAR-3 (%)
0.6784
0.7429
0.6784
0.9863
cell number
2
>2
2
>2
Control
Mitomycin
E
PAR-3 F-actin
a
b
F
PAR-3 intensity
Control
Mitomycin
Cell-cell interface length
G
0.4936
Ratio of PAR-3 in Centre / Outer
Con
Mito
Expt #1
Expt #2
Expt #3
H
ZO-1/GM130
F-actin
i. Control
ii. Mitomycin C
I
Apolar
Polarised
mESC clusters (%)
0.2698
0.3343
Ctrl
Mito
Ctrl
Mito
ZO-1
GM130
J
γ-Tubulin/F-actin
DAPI
i. Control
ii. Mitomycin C
K
Mito
Ctrl
0.2261
2-cell cluster length (X)

**Figure 2**

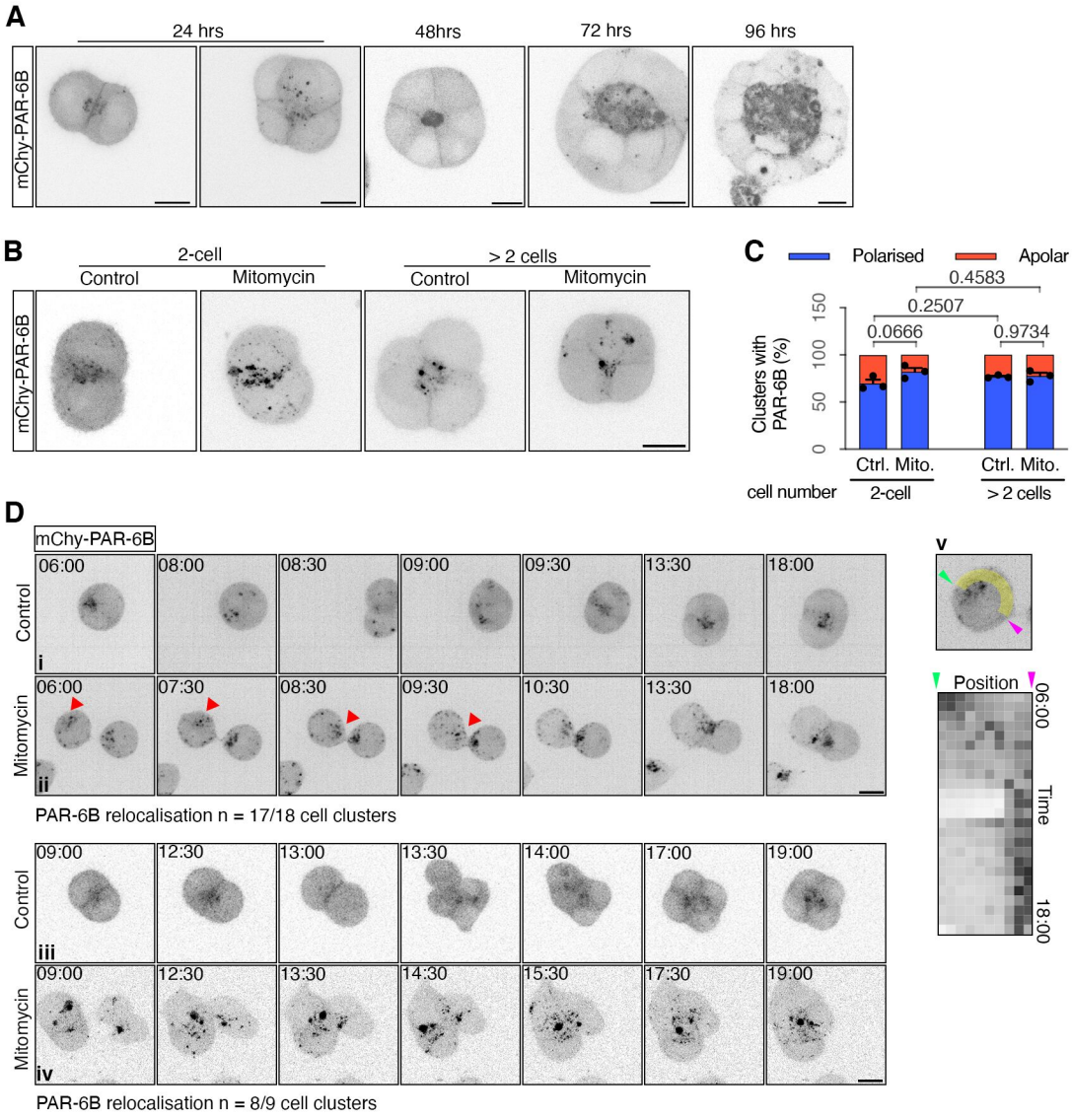
A
24 hrs
48hrs
72 hrs
96 hrs
mChy-PAR-6B
B
2-cell
> 2 cells
Control
Mitomycin
Control
Mitomycin
mChy-PAR-6B
C
Polarised
Apolar
0.4583
0.2507
0.0666
0.9734
Clusters with PAR-6B (%)
0
50
100
150
Ctrl. Mito.
Ctrl. Mito.
cell number
2-cell
> 2 cells
D
mChy-PAR-6B
Control
Mitomycin
06:00
08:00
08:30
09:00
09:30
13:30
18:00
i
06:00
07:30
08:30
09:30
10:30
13:30
18:00
ii
PAR-6B relocalisation n = 17/18 cell clusters
09:00
12:30
13:00
13:30
14:00
17:00
19:00
iii
09:00
12:30
13:30
14:30
15:30
17:30
19:00
iv
PAR-6B relocalisation n = 8/9 cell clusters
v
Position
Time
06:00
18:00

Figure 3

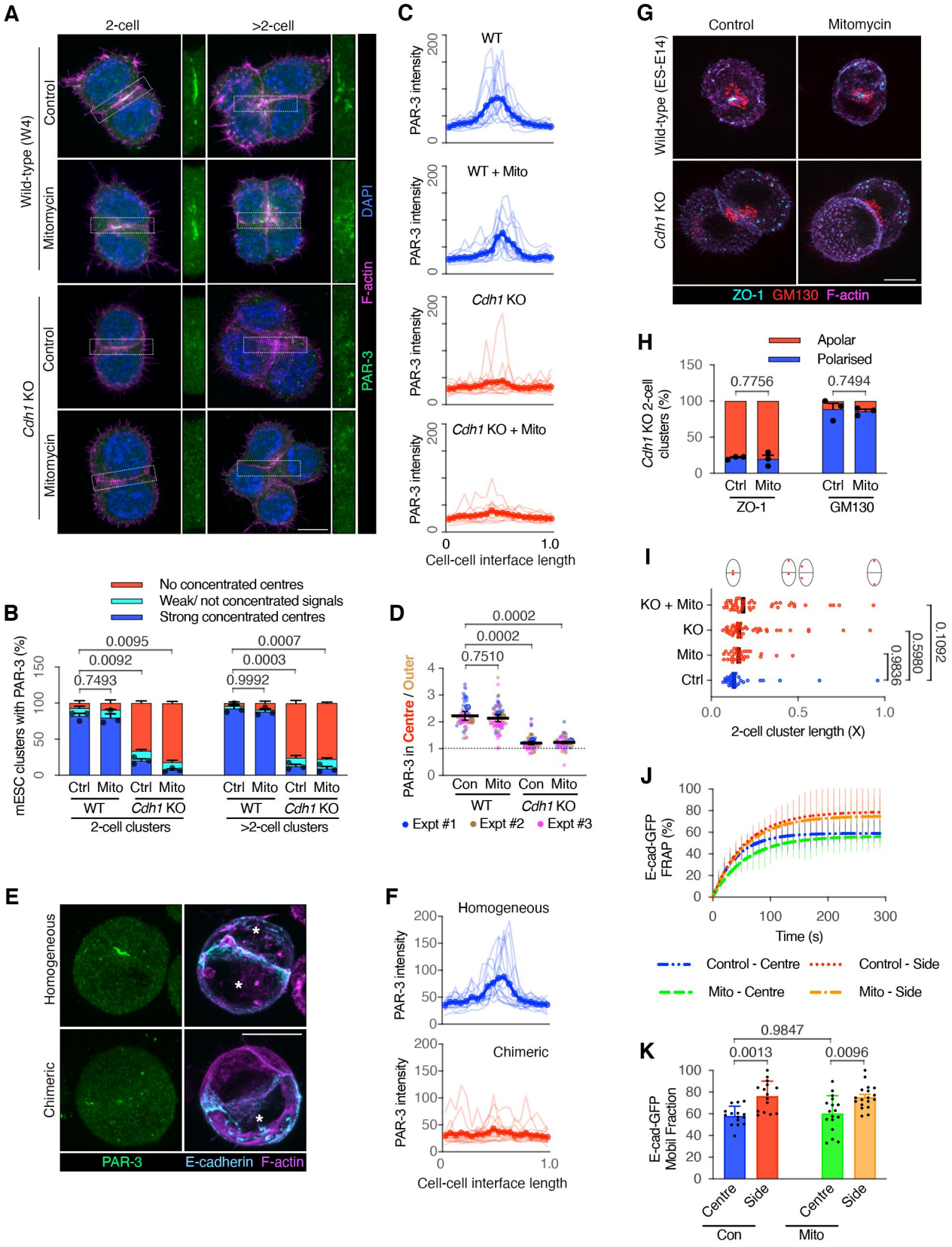
A
2-cell
>2-cell
Wild-type (W4)
Control
Mitomycin
Cdh1 KO
Control
Mitomycin
DAPI
F-actin
PAR-3
C
WT
WT + Mito
Cdh1 KO
Cdh1 KO + Mito
PAR-3 intensity
0
200
0
1.0
Cell-cell interface length
G
Control
Mitomycin
Wild-type (ES-E14)
Cdh1 KO
ZO-1 GM130 F-actin
H
Apolar
Polarised
Cdh1 KO 2-cell clusters (%)
0.7756
0.7494
Ctrl Mito Ctrl Mito
ZO-1
GM130
B
No concentrated centres
Weak/ not concentrated signals
Strong concentrated centres
mESC clusters with PAR-3 (%)
0.0095
0.0092
0.7493
0.0007
0.0003
0.9992
Ctrl Mito Ctrl Mito
WT
Cdh1 KO
2-cell clusters
>2-cell clusters
D
0.0002
0.0002
0.7510
PAR-3 in Centre / Outer
Con Mito Con Mito
WT
Cdh1 KO
Expt #1
Expt #2
Expt #3
I
KO + Mito
KO
Mito
Ctrl
0.1092
0.5980
0.9836
0.0
0.5
1.0
2-cell cluster length (X)
J
E-cad-GFP FRAP (%)
Time (s)
Control - Centre
Control - Side
Mito - Centre
Mito - Side
E
Homogeneous
Chimeric
PAR-3
E-cadherin F-actin
F
Homogeneous
Chimeric
PAR-3 intensity
Cell-cell interface length
K
0.9847
0.0013
0.0096
E-cad-GFP Mobil Fraction
Centre Side Centre Side
Con
Mito

Figure 4

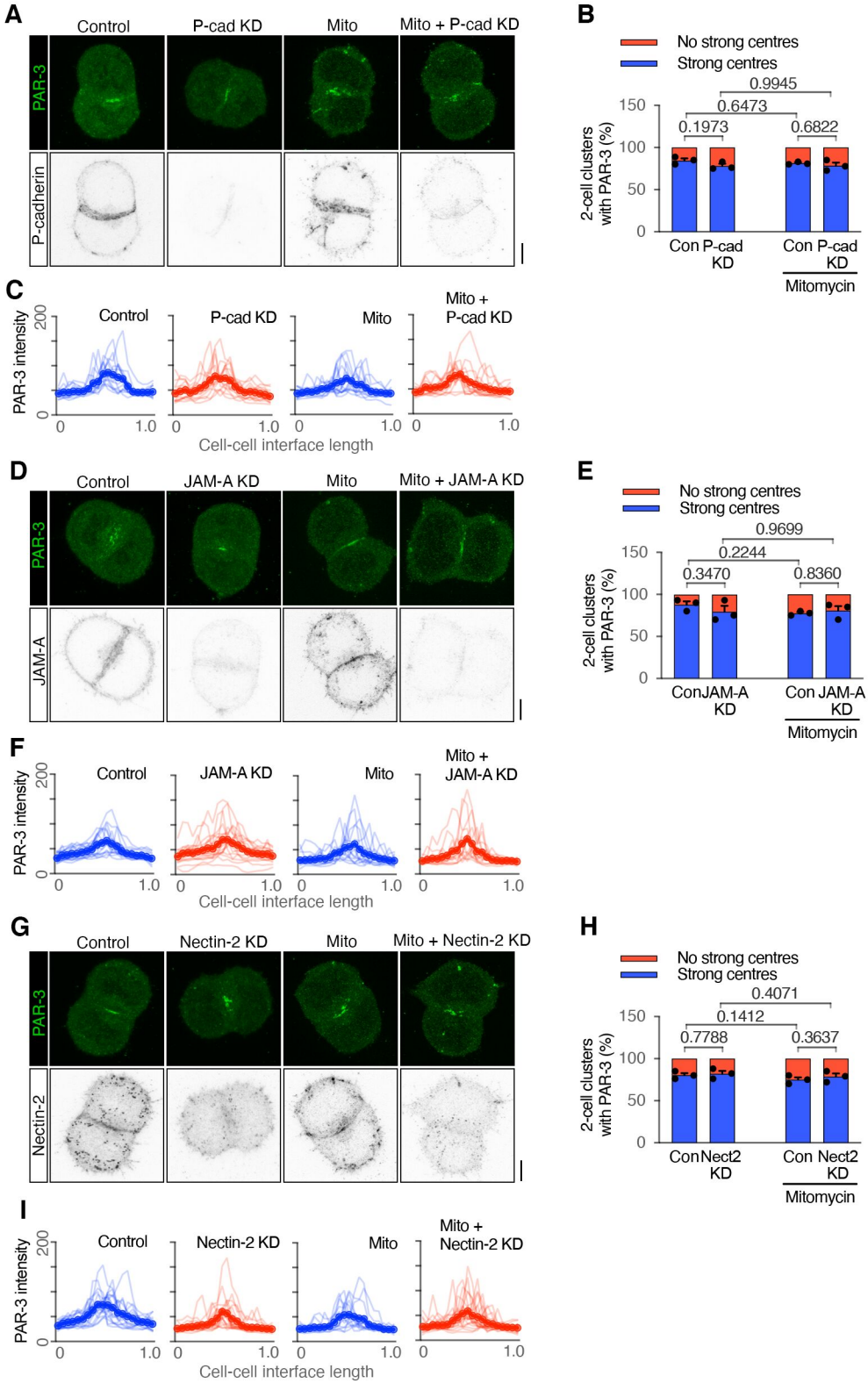
A
Control
P-cad KD
Mito
Mito + P-cad KD
PAR-3
P-cadherin
B
No strong centres
Strong centres
0.9945
0.6473
0.1973
0.6822
2-cell clusters with PAR-3 (%)
150
100
50
0
Con
P-cad KD
Con
P-cad KD
Mitomycin
C
Control
P-cad KD
Mito
Mito + P-cad KD
PAR-3 intensity
200
0
1.0
Cell-cell interface length
D
Control
JAM-A KD
Mito
Mito + JAM-A KD
PAR-3
JAM-A
E
No strong centres
Strong centres
0.9699
0.2244
0.3470
0.8360
2-cell clusters with PAR-3 (%)
Con
JAM-A KD
Con
JAM-A KD
Mitomycin
F
Control
JAM-A KD
Mito
Mito + JAM-A KD
PAR-3 intensity
Cell-cell interface length
G
Control
Nectin-2 KD
Mito
Mito + Nectin-2 KD
PAR-3
Nectin-2
H
No strong centres
Strong centres
0.4071
0.1412
0.7788
0.3637
2-cell clusters with PAR-3 (%)
Con
Nect2 KD
Con
Nect2 KD
Mitomycin
I
Control
Nectin-2 KD
Mito
Mito + Nectin-2 KD
PAR-3 intensity
Cell-cell interface length

**Figure 5**

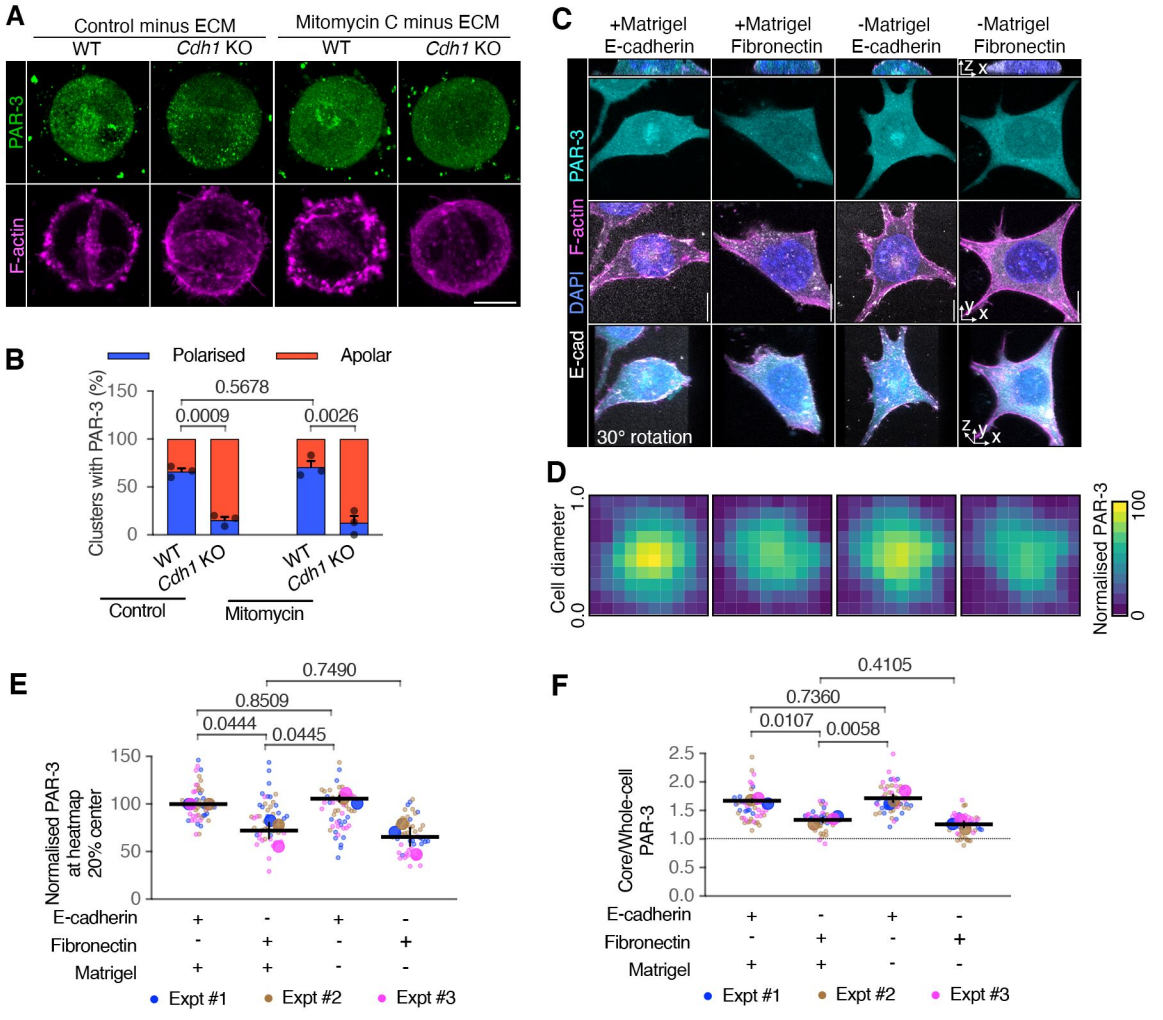
A
Control minus ECM
Mitomycin C minus ECM
WT
Cdh1 KO
WT
Cdh1 KO
PAR-3
F-actin
B
Polarised
Apolar
Clusters with PAR-3 (%)
150
100
50
0
0.5678
0.0009
0.0026
WT
Cdh1 KO
WT
Cdh1 KO
Control
Mitomycin
C
+Matrigel
E-cadherin
+Matrigel
Fibronectin
-Matrigel
E-cadherin
-Matrigel
Fibronectin
PAR-3
F-actin
DAPI
E-cad
30° rotation
D
Cell diameter
1.0
0.0
Normalised PAR-3
100
0
E
0.7490
0.8509
0.0444
0.0445
Normalised PAR-3 at heatmap 20% center
150
100
50
0
E-cadherin + - + -
Fibronectin - + - +
Matrigel + + - -
Expt #1
Expt #2
Expt #3
F
0.4105
0.7360
0.0107
0.0058
Core/Whole-cell PAR-3
2.5
2.0
1.5
1.0
0.5
0.0
E-cadherin + - + -
Fibronectin - + - +
Matrigel + + - -
Expt #1
Expt #2
Expt #3

Figure 6

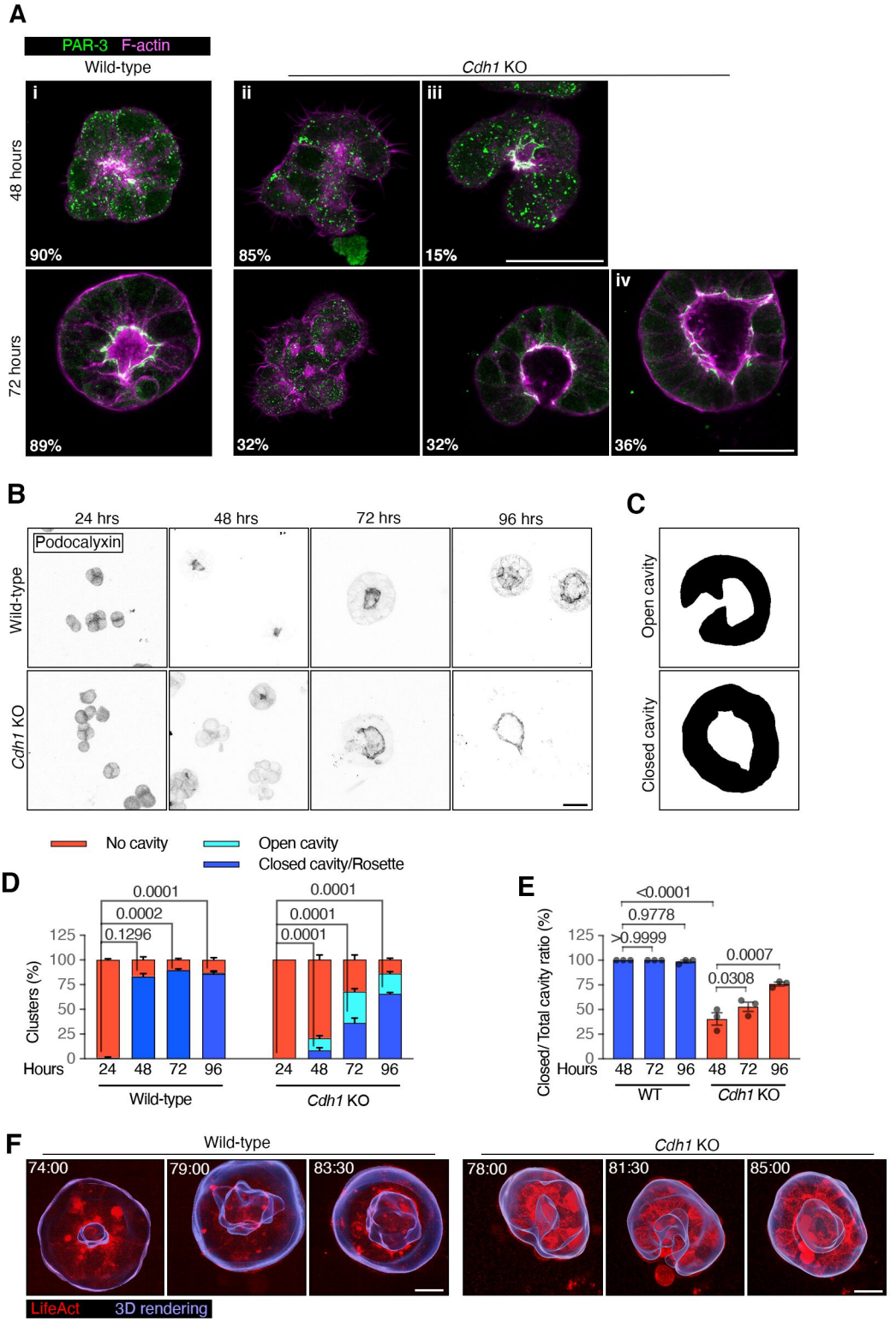
A
PAR-3 F-actin
Wild-type
Cdh1 KO
i
ii
iii
iv
48 hours
72 hours
90%
85%
15%
89%
32%
32%
36%
B
24 hrs
48 hrs
72 hrs
96 hrs
Podocalyxin
Wild-type
Cdh1 KO
C
Open cavity
Closed cavity
No cavity
Open cavity
Closed cavity/Rosette
D
Clusters (%)
Hours
Wild-type
Cdh1 KO
0.0001
0.0002
0.1296
0.0001
0.0001
0.0001
E
Closed/ Total cavity ratio (%)
Hours
WT
Cdh1 KO
<0.0001
0.9778
>0.9999
0.0007
0.0308
F
Wild-type
Cdh1 KO
74:00
79:00
83:30
78:00
81:30
85:00
LifeAct
3D rendering

**Figure 7**

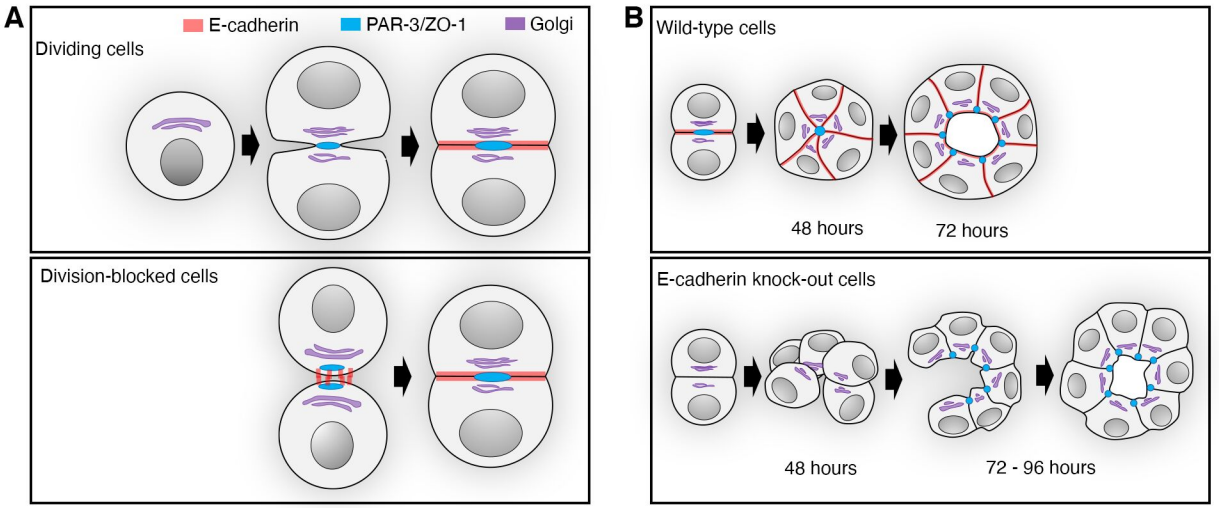
A
E-cadherin
PAR-3/ZO-1
Golgi
Dividing cells
Division-blocked cells
B
Wild-type cells
48 hours
72 hours
E-cadherin knock-out cells
48 hours
72 - 96 hours